Chapter 3

Synthesis Procedure and Structural, Optical, Electrical Characterization of SnS Nanostructured Materials

3.1. Structural and Optical Characterization of SnS Nanoparticles Grown by Chemical Reduction Route

SnS nanoparticles are synthesized by simple chemical reduction route with the variation of growth time (3h to 14h) using tetrahydrofuran (THF) as medium. Sodium borohydride ($NaBH_4$) acts as reducing agent. The as prepared samples are studied structurally by transmission electron microscopy (TEM) and X-ray diffraction (XRD). Optical characterization of the nanoparticles is done by optical absorption (UV-vis) and photoluminescence (PL) spectroscopy. The crystallite size increases with increase of growth time. A decrease in band gap energy is observed with increase of growth time. Photoluminescence spectra determine the defect states of the samples. Atomic force microscopy (AFM) analysis shows that roughness is small for lower growth time sample.

3.1.1. Experimental section

Tin sulphide (SnS) nanoparticles were prepared by cost effective chemical reduction route. For this purpose Tin (II) chloride ($SnCl_2.2H_2O$) and sulfur powder (S) were taken in analytic grade as tin and sulfur sources respectively and THF used as a reaction medium. Sodium Borohydride (0.074 gm) were taken as a reducing agent. Different samples were synthesized by varying growth time. At first 0.45 gm of $SnCl_2.2H_2O$ was mixed in 50 ml THF taken in a beaker. After stirring, sulfur powder (0.064 gm) was mixed with the solution. Finally, Sodium Borohydride was added into the solution which was under stirring. The solution turns deep brown which indicates the formation of tin sulfide nanoparticles. The

reactions were carried out at 27 ^{0}C under different growth times as 3 hrs, 7 hrs, and 14 hrs at a constant speed using magnetic stirrer. The final products were centrifuged washed with deionised water for some times and dried at 50 ^{0}C for few hours. The chemical reaction to grow SnS nanocrystals are

$$SnCl_2 = Sn^{2+} + 2Cl^{2-},$$

$$NaBH_4 + 2Cl^{2-} = NaCl + B_2H_6 + 2H + 2e^{2-}$$

$$2H + S = H_2S,$$

$$H_2S + Sn^{2+} + 2e^{2-} = SnS + H_2$$

The X-ray diffraction (XRD) pattern of the as-prepared SnS nanoparticles were recorded by a X-ray diffractometer (miniflex II, desktop-X-ray diffractometer) using Cu kα radiation of wavelength λ = 1.5405 Å for 2θ varying from 20° to 70°. The morphological structure of the grown SnS NPs was characterized by transmission electron microscope using a JEOL-JEM2010 operating at 200 kV. Selected area electron diffraction (SAED) pattern of the grown samples were also characterized. Optical absorption study of the dispersed samples was studied in the wavelength range of 300–700 nm using a Shimadzu Pharmaspec 1700 UV–Vis Spectrophotometer. PL spectra of the dispersed SnS NPs are recorded using Perkin Elmer LS 55 Fluorescence Spectrophotometer.

3.1.2. Results and discussion

3.1.2.1. XRD study

XRD pattern of the synthesized SnS NPs are shown in Fig. 3.1. The diffraction peaks confirm that the materials are in mixture of orthorhombic and hexagonal phases as compared with JCPDS data (JCPDS Card No: 39-0354). The broadening of the XRD peaks of the samples signified the formation of SnS NPs. Particle size D of the nancrystals was calculated using Debye Scherrer's formula:

$$D = \frac{0.9\lambda}{\beta_{1/2} COS\theta} \qquad (3.1.1)$$

Where, λ is the wavelength of the incident X-rays which is 1.5405 Å, β1/2 is the full width half maximum (FWHM), 2θ is the diffraction angle. With increase of growth time half width of the peak decreases which indicates that crystalline size of SnS nanostructure increases.

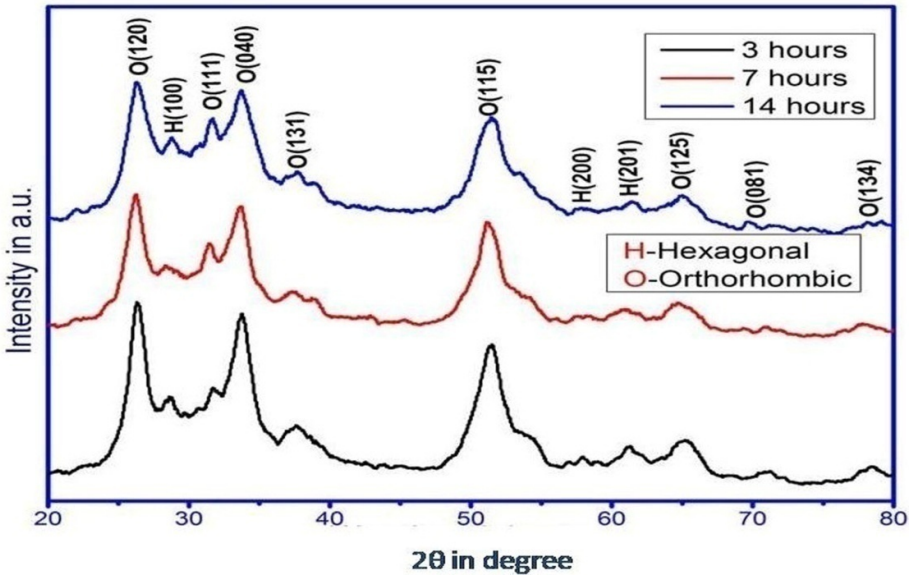

Fig. 3.1. XRD pattern of as prepared SnS NPs

3.1.2.2. TEM and SEM study

The TEM and SAED pattern of as synthesized time variation SnS nancrystals are depicted in fig. 3.2. The average diameter of the particles are determined from the TEM micrograph and found to be ~ 20 nm, ~30 nm, ~180 nm for samples grown under 3 hrs, 7 hrs and 14 hrs respectively. So it confirms that the diameter of the nanocrystals belongs to the weak confinement region since the Bohr's radius of the SnS crystal is about 9.5 nm. From micrograph pattern it is clearly observed that with increase of growth time the crystal size increases obeying the process called Ostwald Ripening [191]. Again, we see that the size of the particles is growing in a particular direction for large time (14 hrs) reaction. This could be due to heterogeneous nucleation process. Also from SAED pattern it is observed that with increase of growth time spots reduces to ring pattern which confirm that single crystallinity is reduced.

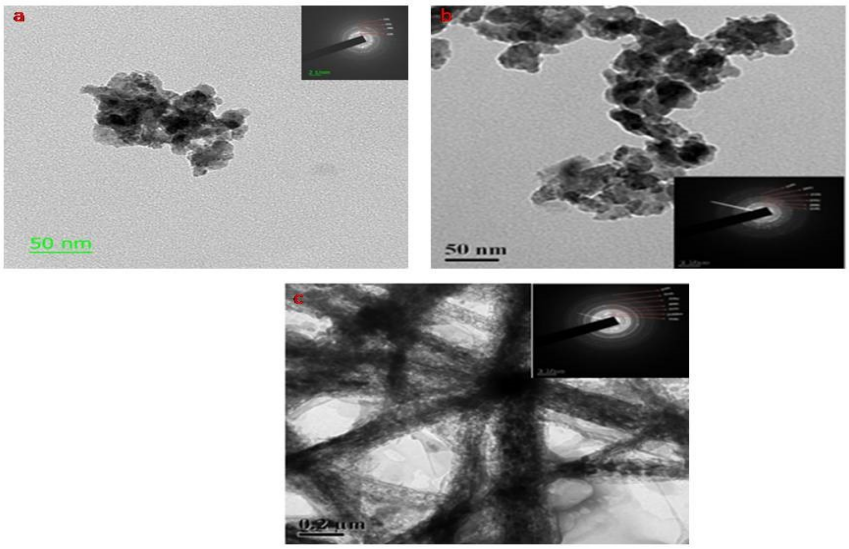

Fig. 3.2. TEM image and SAED (inset) pattern of (a) 3 h sample, (b) 7 h sample, (c) 14 h sample

SEM image gives the information about surface morphology, orientation of atomic structure, crystalline nature of the materials. Fig. 3.3 indicates the SEM image of SnS nanostructure for 3 hrs, 7 hrs and 14 hrs. From the image we see that the particles density on the surface increases with increase of growth time. It consists of particle grains with precise uniformity.

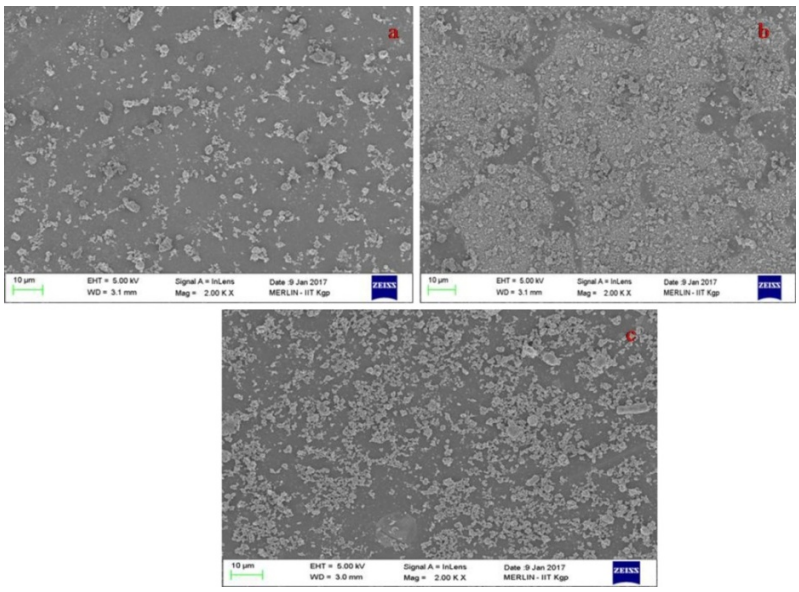

Fig. 3.3. FESEM of (a)3 h SnS, (b) 7 h SnS, (c) 14 h SnS

3.1.2.3. EDX analysis

EDX analysis indicates elemental compositions of tin sulfide (SnS) nanoparticles. It provides information about atomic percentage of the elements of Sn and S in SnS nanocrystal. From EDX analysis we see that the atomic percentage of S is more than Sn for all samples as shown in fig. 3.4. The Sn/S variation is small for different hours grown sample. Since the stochiometric deviation is small the change in band gap energy is due to quantum confinement.

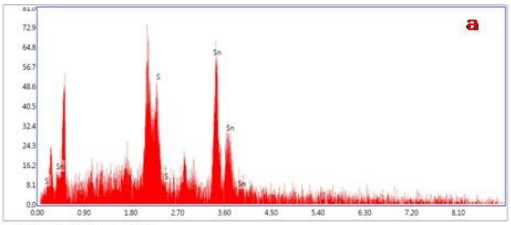

b

eZAF Smart Quant Results

Element	Weight %	Atomic %	Net Int.	Error %	Kratio	Z	R	A	F
SK	24.30	54.30	164.61	9.73	0.29	1.31	0.88	0.89	1.02
SnL	75.70	45.70	119.35	14.50	0.68	0.9	1.05	0.99	1.02

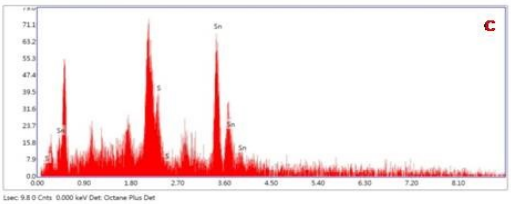

d

eZAF Smart Quant Results

Element	Weight %	Atomic %	Net Int.	Error %	Kratio	Z	R	A	F
SK	22.84	52.29	137.94	9.21	0.27	1.30	0.88	0.89	1.02
SnL	77.16	47.71	108.78	18.01	0.70	0.89	1.31	0.99	1.02

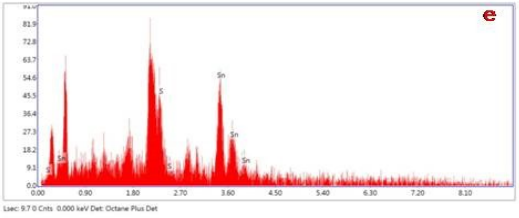

f

eZAF Smart Quant Results

Element	Weight %	Atomic %	Net Int.	Error %	Kratio	Z	R	A	F
SK	28.99	60.18	174.64	9.13	0.34	1.28	0.89	0.9	1.02
SnL	71.01	39.82	98.54	18.18	0.63	0.88	1.06	0.99	1.02

Fig. 3.4. (a) EDAX pattern of 3 h SnS, (b) atomic ratio of Sn and S of 3 h SnS, (c) EDAX pattern of 7 h SnS, (d) atomic ratio of Sn and S of 7 h SnS, (e) EDAX pattern of 14 h SnS, (f) atomic ratio of Sn and S of 14 h SnS.

3.1.2.4. Optical properties

UV-VIS spectroscopy measurement was used to determine optical properties of the as- prepared SnS nanocrystals and the band gap. Fig. 3.5 clearly demonstrates the absorbance spectrum of SnS nanoparticles with growth time 3 hrs, 7 hrs and 14 hrs. Optical absorption coefficient has been determined in wavelength range from 200-900 nm. It is observed that the

SnS nanocrystals have strong absorption range from NIR to UV. The band gap of as-prepared SnS nanoparticles are determined using the following releation:

$$(\alpha h\nu)^2 = C\,(h\nu - E_g) \qquad (3.1.2)$$

Where C is a constant, E_g is the band gap energy of the material, α is the absorption coefficient of the material, and ν is the frequency of light used. Plot of photon energy (hυ) with $(\alpha h\upsilon)^2$ is depicted in fig. 3.6. The estimated band gaps are 2.28 eV, 2.15 eV, and 1.79 eV for samples with different growth time for 3 hrs, 7 hrs and 14 hrs respectively. These band gaps are large compared to the bulk band gap energy (1.3 eV). Therefore quantum confinement effect [64] takes place.

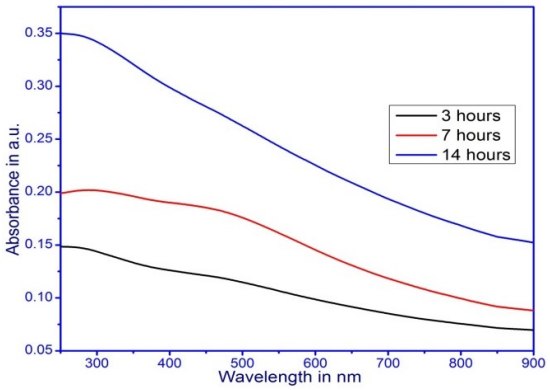

Fig. 3.5.

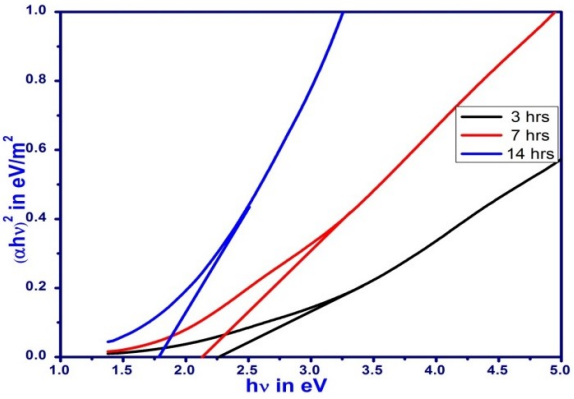

Fig. 3.6.

Fig. 3.5. Optical absorbance spectra of SnS nanoparticles grown at different time.

Fig. 3.6. Graph for band gap determination of SnS nanoparticles.

3.1.2.5. Photoluminescence spectroscopy

PL study investigates the defect or impurity state of a material. Room temperature PL spectrum of as- synthesized SnS nanocrystals dissolved in ethanol is shown in fig. 3.7. As the particle size increases with increase of growth time, the emission peaks shift towards higher wavelength region. The increase of particle size leads to decrease of band gap. As a result a red shift is observed with increase of growth time of SnS nanocrystals. The emissions cannot be attributed to band edge luminescence of SnS samples since emission peaks are occurring

lower than the band gap of SnS nanocrystals. Peaks are possibly arising due to the defect states of sulfur vacancies [97].

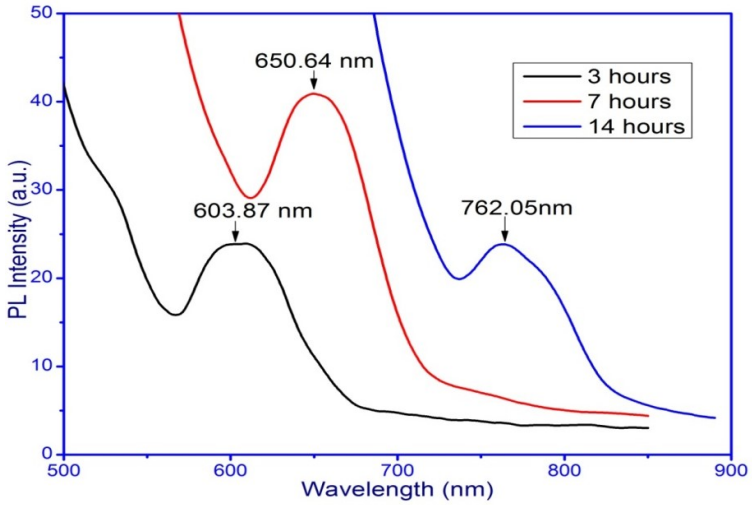

Fig. 3.7. PL spectra of SnS NPs.

3.1.2.6. AFM study

Fig. 3.8 shows 3-dimensional view of AFM images of different SnS nanocrystals deposited as film on glass. The measured values of roughness were 7.67 nm, 25.4 nm, and 39.6 nm for samples grown for 3 hrs, 7 hrs and 14 hrs respectively.

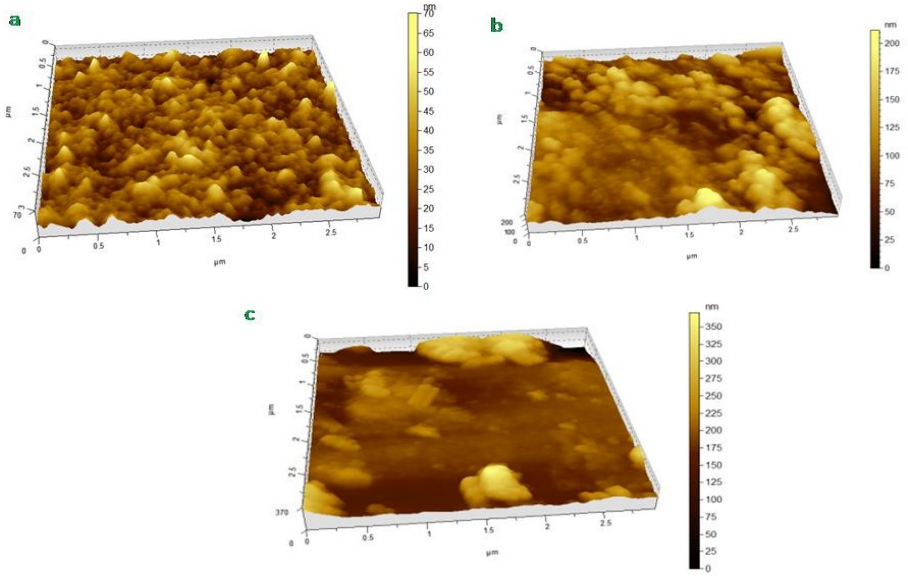

Fig. 3.8. 3-D AFM image of (a) 3 h SnS, (b) 7 h SnS, (c) 14 h SnS.

Thus surface roughness increases with increase of growth time. With increase of growth time the crystal size increase i.e surface to volume ratio decreases resulting in the increase of surface roughness.

Table 3.1

Summarization of characterization for all samples prepared by chemical reduction route

Sample	Pattern	Size from TEM image (nm)	Band gap from UV-VIS spectroscopy (eV)	PL peak position (nm)	Atomic percentage from EDS		Roughness of SnS film on glass from AFM (nm)
					Sn	S	
SnS -3 hour	Particle	~20	2.28	603.87	54.30	45.70	7.67
SnS -7 hour	Particle	~30	2.15	650.64	52.29	47.71	25.4
SnS -14 hour	Rod	~180	1.79	762.05	60.18	39.82	39.6

3.1.3. Conclusion

SnS nanoparicles are grown in a cost effective method. The nanoparicles are characterized structurally and optically. XRD result shows that the as prepared nanoparticles are the mixture of hexagonal and orthorhombic phase. The film roughness increases with increase of size of particles. The TEM micrograph indicates the formation of particles in a particular direction for large time (14 hrs) reaction. It is confirmed that the size and shape of SnS NPs normally depend on the growth time. Optical study shows that the band gap decreases with increase of growth time. Therefore, the result shows weak confinement effect.

3.2. Structural and Optical Characterization of SnS Nanoparticles Grown at Room Temperature using Wet Chemical Precipitation Method

SnS nanoparticles were synthesized by simple and cost effective precipitation method. The prepared nanoparticles were characterized structurally by X-Ray diffraction (XRD), transmission electron microscopy (TEM), field emission scanning electron microscopy (FESEM) and atomic force microscopy (AFM). The as synthesized NPs were also characterized optically by optical absorption spectroscopy (UV-vis) and photoluminescence spectroscopy (PL). XRD image shows particles are orthorhombic structure. The TEM image indicates that grown nanoparticles are spherical in shape and crystallite size is about 20 nm. SAED pattern reveals the good crystalline nature of nanoparticles. An increase in the band gap was observed compared to bulk SnS (1.3 eV) which confirmed the formation of NPs. Optical absorption study determines the band gap of the grown sample is about 1.76 eV. PL spectra of SnS show an emission peak at 698.79 nm.

3.2.1. Experimental section

The SnS nanoparticle has been prepared by Precipitation method. In a typical synthesis 0.5 mole of tin chloride (4.51g, in 40 ml deionized water) and 0.5 mole of sodium sulfide (1.51g, in 40 ml deionized water) was used in the analytical grade as sources of tin and sulphur respectively. Briefly, at first $SnCl_2.2H_2O$ and Na_2S were taken individually in the deionized water kept in a beaker. Stirring was continuing using a magnetic stirrer until both the solutions dissolved well. After that 5 ml of TEA which acts as a catalytic (triethanolamine) was mixed to the $SnCl_2.2H_2O$ solution. Finally, both solutions were mixed together and stirring at a speed 700 r.p.m. The solution was turned into dark brown black in color and colloidal form which indicates that SnS nanoparticles have been formed. The obtained black

solid precipitates were centrifuged and washed with deionized water for several times and dried at room temperature for two days for further characterization.

For structural characterization, XRD patterns of the as prepared sample was recorded in Rigaku-miniflex electro diffractometer using CuK_{α} radiation (λ=1.5405A°) in the range $20^0 < 2\theta < 70^0$. TEM and SAED of SnS nanocrystals were performed using JEOL-JEM-200 opreating at 200 KV. FESEM analysis of the nanocrystals was obtained using Zeiss SEM operating at 5 kV. Mechanical strength in surface of prepared sample was carried out through Atomic Force Macrograph (AFM). Optical absorption data was taken from Shimadzu-Pharmaspec-1700 UV-VIS within 300-900 nm. Room temperature photoluminescence spectroscopies of SnS nanoparticles were determined using PerkinElmer LS 55 Fluorescence Spectrometer.

3.2.2. Results and discussion

3.2.2.1. XRD studies

The XRD pattern of as- synthesized nanoparticles prepared by precipitation method is shown in fig.3.9. All the peaks are clearly identified and perfectly matched with orthorhombic structure as comparing with JCPDS data. The lattice parameters of SnS nanocrystals are a= 4.328Å, b= 11.19Å, c= 3.978Å. The planes [120], [101], [111], [131], [141], [211] and [122] represent different reflecting crystal planes of SnS nanocrystals.

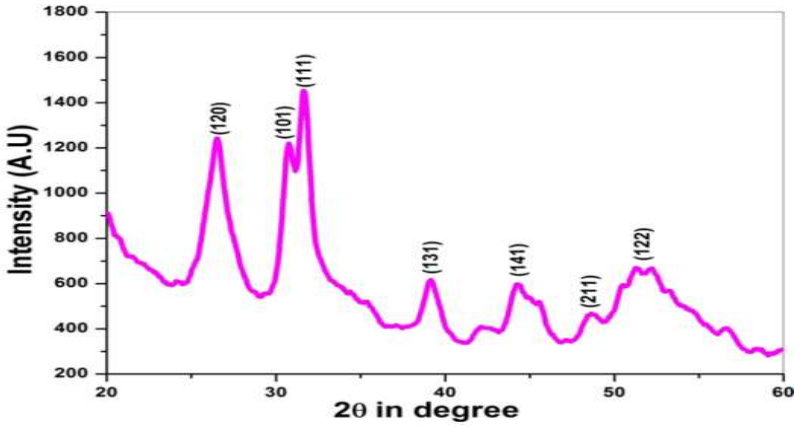

Fig. 3.9. XRD pattern of SnS nanoparticles grown at room temperature

No impurity peaks of source materials are observed. The broadening of the XRD peaks of the sample indicates that SnS nanoparticles have been formed. The Particle size is calculated from Scherer's formula. The (120) plane was used to determine the size of the SnS nanocrystals using Scherer's formula. The crystalline size of the as synthesized sample is approximately 13nm.

3.2.2.2. TEM and ED studies

The morphology of the obtained nanocrystals was further certified by transmission electron microscopy (TEM). Fig. 3.10 shows TEM image and the corresponding SAED pattern of grown SnS nanocrystals. It is observed that chain-like spherical nanoparticles have been formed. The approximate diameter of prepared SnS nanocrystals is about 20 nm [46]. The SAED pattern consists of diffraction rings together with bright spots confirms well-crystalline nature of SnS nanomaterial and hence TEM as well as SAED images perfectly agree with the XRD results.

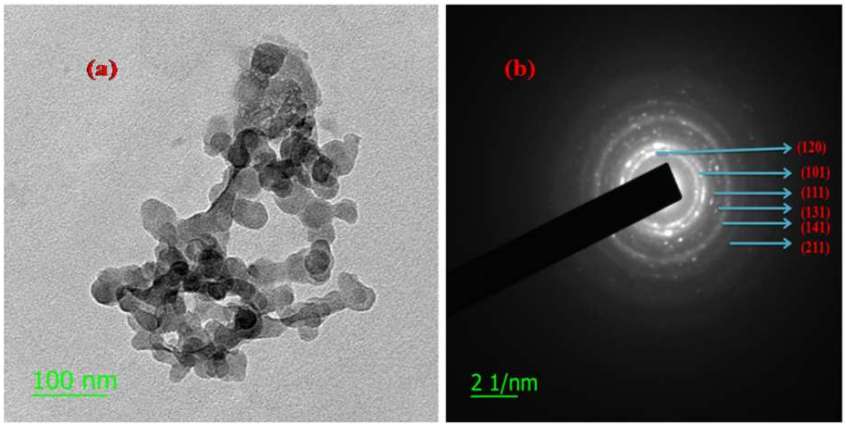

Fig. 3.10. (a) The TEM image of SnS nanoparticles ; (b) SAED pattern of SnS nanoparticles at R.T.

3.2.2.3. FESEM study

Surface morphology, orientation of atomic structure and crystalline nature of the materials was studied by FESEM. Fig.3.11 shows FESEM image of as synthesized SnS nanomaterial. From FESEM image it is clear that the particles are in agglomerated state due

to their small crystal size and high surface energy. FESEM result also support the TEM result.

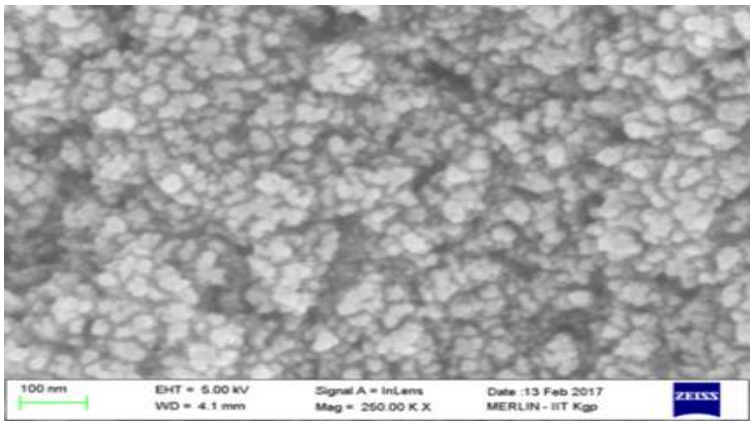

Fig. 3.11. FESEM image of SnS nanoparticles at R.T.

3.2.2.4. AFM analysis

The mechanical strength of surface morphology can be studied from AFM analysis. AFM image is shown in Fig.3.12. It is observed that the SnS nanocrystals consist of spherical grain with better uniformity. The surface roughness of SnS nanocrystals is very small and it is approximately 7.39 nm.

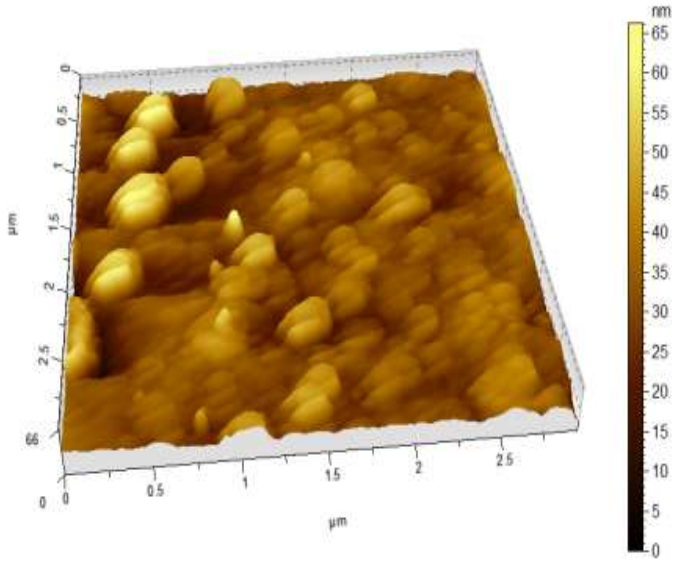

Fig. 3.12. AFM image of as prepared SnS at R.T.

3.2.2.5. Optical absorption study

UV-VIS spectroscopy measurement was done to determine the band structure and optical properties of the as-Prepared SnS nanocrystals dispersed in ethanol. The absorption spectrum of SnS is depicted in fig. 3.13. The optical absorption coefficient is determined in the wavelength range of 300–900 nm. The variation of $(\alpha h\nu)^2$ vs. photon energy hν is shown in fig.3.14.The band gap energy of the as-synthesized nanocrystals is about 1.76 eV. The band gap energy is determined using the relation

$$(\alpha h\nu)^2 = C\,(h\nu - E_g) \qquad (3.2.1)$$

Where c is constant, E_g is the band gap energy of the material and α is the optical absorption coefficient of the material. This red emission indicates that the SnS nanoparticle can be used as red light emitter and in other optical devices. Therefore a blue shift of ~ 0.46 eV is observed as compared to the bulk SnS nanocrystals which are due to quantum confinement effect of electron in SnS nanocrystals [97].

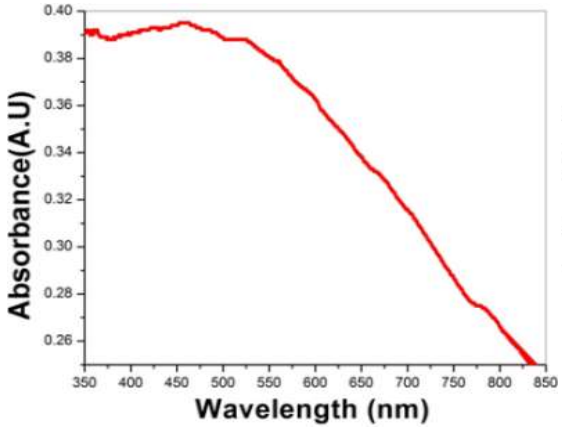

Fig. 3.13. UV–Vis spectra of SnS at R.T

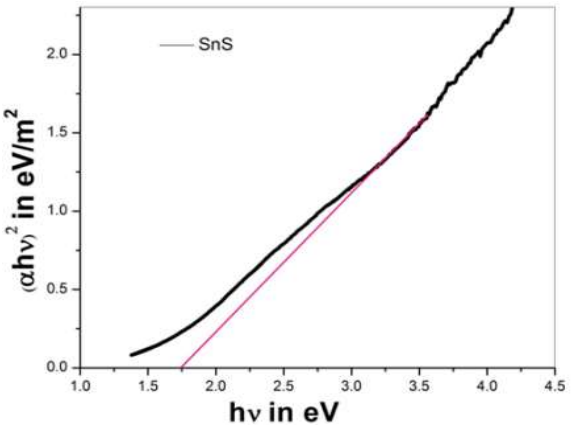

Fig. 3.14. Band gap determination graph

3.2.2.6. Photoluminescence study

Photoluminescence (PL) study of SnS nanocrystals dispersed in ethanol is done at room temperature with excitation wavelength at 550 nm as shown in fig. 3.15. PL spectrum consists of one strong peak at 698.79 nm (1.77eV) which is due to the band to band transition

of SnS nanocrystals. This is attributed due to band to band transition and defect states like sulfur as well tin ion vacancies. Therefore a large blue shift indicates quenching effect of charge carriers of SnS nanocrystals. In present PL study the strong emission peak at 698.79 nm is arising from band edge and defect state of sulfur ion vacancies [192]. The broadening of PL peak indicates that different size crystals have been formed.

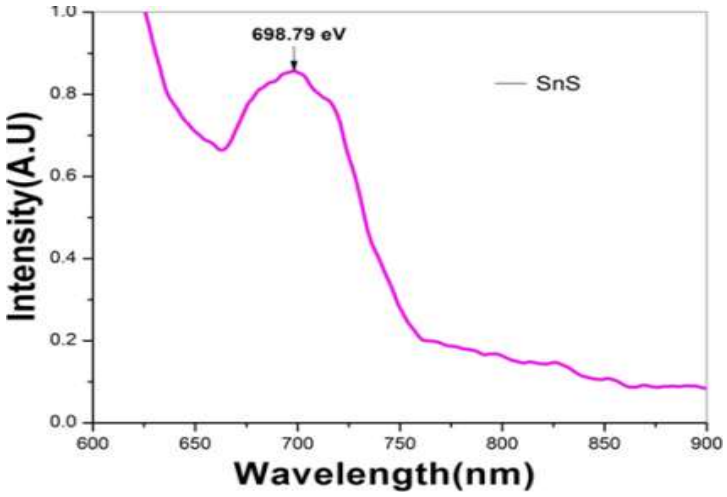

Fig. 3.15. PL spectra of prepared SnS grown at room temperature

Table 3.2

Summarization table

Sample	**Pattern**	**Crystal Size from TEM image (nm)**	**Band gap from UV-VIS spectroscopy (eV)**	**PL peak position (nm)**	**Surface roughness of SnS film on glass from AFM (nm)**
SnS at R.T	Chain-like Particle	~20	1.76	698.79	7.39

3.2.3. Conclusion

SnS nanocrystals have been prepared through precipitation method using TEA. XRD image shows that the particles are orthorhombic structure. The TEM image shows that particles are chain-like shape and crystal size is about 20 nm. FESEM result also support the TEM result. AFM image shows that the surface roughness of the as prepared SnS nanocrystals is about 7.39 nm. Optical absorption study determines the band gap of the grown sample is about 1.76 eV. PL spectra of SnS shows an emission peak at 698.79 nm which is due to band to band transition. The optical studies confirmed that the as prepared nanocrystals show a strong red emission. Thus the increase of band gap is due to quantum confinement effect.

3.3. Structural, Optical and Electrical Characterization of SnS Nanoparticles Grown by Varying Growth Temperature through Wet Chemical Precipitation Method

SnS nanocrystals were synthesized by simple wet chemical precipitation method. XRD results shows that the crystals are orthorhombic in phase. TEM images indicate that the grain sizes are almost spherical within the range 5 nm to 10 nm. Crystalline natures of the samples were confirmed by HRTEM. AFM analysis shows that surface roughness were found to be moderate. EDAX analysis revealed that the samples are maintained good stoichiometric ratio of Sn/S. From UV–Vis absorption spectra it is evident that SnS nanocrystals are good absorbing materials for solar light. PL spectra indicate a red shift of SnS nanocrystals occurred with increase growth temperature. Time correlated single photon counting (TCSPC) measurements revealed that PL decay life times are in the order of picosecond. The temperature varying SnS nanocrystals were p-type in nature with electrical conductivities were ranging from 0.020 to 0.037 Ohm^{-1} cm^{-1} and carrier concentrations were 7.05×10^{13} cm^{-3} to 1.54×10^{14} cm^{-3}. Carriers drift mobilities were found to be high compared to the reported results. Therefore, SnS nanocrystals having low resistivity, higher drift mobility, higher carrier concentrations, small PL decay life time and high absorption coefficient are suitable for the fabrication of optoelectronic devices.

3.3.1. Experimental section

Chemical method has been followed to grow SnS nanoparticle in different bath temperature. In this synthesis 2.25 gm $SnCl_2.2H_2O$ which is the source of tin was dissolved in 40 ml deionized water. Then 5 ml triethylamine was added to the tin chloride solution under magnetic stirring. Under this condition 40 ml (0.78 gm Na_2S. XH_2O in 40ml deionised water) sodium sulfide solution which is the source of sulfur added drop wise into the tin chloride solution. Stirring was continued for 2 hours in different bath temperature at 14 ^{0}C, 30 ^{0}C and

70 ^{0}C. The solutions were turned into brown black in color. The obtained precipitates were centrifuged and washed with ethanol and deionized water for several times and dried at 40 ^{0}C for two days for structural and optical properties. To study the electrical properties of SnS nanocrystals, a nanofilm of the different samples has been grown on the glasses from the dispersed SnS nanoparticles in ethanol. Silver paste has been drawn as electrode on the glass for electrical characterization.

X-ray diffraction (XRD) measurements were performed by Bruker Axs D2 phaser SSD160 with Cu-kα radiation (λ=1.5405Å) in the range of 20° to 70°. Raman spectroscopy (Renishaw invia Raman microscope) was also carried out to identify the phases of the as prepared samples with an excitation wavelength of 532nm. Transmission electron microscopy and HRTEM were carried out by JEOL JEM200 operating at 200KV. The surface morphology of the grown samples has been characterized by FESEM using ZEISS MERLIN6105. The Surface roughnesses were measured by 5500 AFM (N9410S). The stochiometric analyses were performed by energy dispersive analysis of X-rays (EDAX).UV-VIS absorption spectra of as prepared samples were measured by Shimadzu- Pharmaspec-1700 visible and ultraviolet spectrophotometer in the wavelength range 200nm-900nm at room temperature. PL spectra of as prepared SnS were obtained by Perkin Elmer LS55 Fluorescence Spectrometer. Time-Correlated Single Photon Counting (TCSPC) of the samples was performed by Delta flex-01-DD. Finally, electrical characterization of the nanofilm samples was characterized by ezHEMS nano magnetic instrument.

3.3.2. Results and discussion

3.3.2.1. Structural study using XRD and Raman spectroscopy

X- ray diffraction pattern of 14^{0}C SnS, 30^{0}C SnS and 70^{0}C SnS are presented in fig. 3.16(a). XRD peaks are obtained at 26.49^0, 29.74^0, 31.62^0, 33.43^0, 39.09^0, 44.31^0, 51.68^0, and 64.55^0 indexed as (120), (101), (111), (040), (131), (141), (151) and (080) diffraction planes.

All these diffraction planes are perfectly matched with JCPDS data (JCPDS card no: 39-0354) which can be assigned as orthorhombic crystal structure of SnS with lattice parameters $a = 0.432, b = 1.121$ and $c = 0.399$ nm. No impurity peaks were observed in the XRD image.

The Raman spectroscopic measurements have been also performed to study the structural phases of as-prepared SnS in the range of 100-500 cm^{-1} at room temperature is shown in fig. 3.16(b). Raman spectra show three prominent peaks for all samples around 165 cm^{-1}, 185 cm^{-1}, 231 cm^{-1} and one of the weak intense peaks at 317 cm^{-1}. Among them the most intense peak is at 185 cm^{-1}. According to the literatures, peak presented at 165 cm^{-1}, 185 cm^{-1} and 231 cm^{-1} can be attributed as orthorhombic crystal phase of SnS [193-194]. However, the peak at 317 cm^{-1} is very weak which may be due to the presence of another phase SnS_2 in small amount [195]. This result may be due to the growth technique. The Raman mode at 185 cm^{-1} and 231 cm^{-1} are assigned to the A_g mode whereas the peak at 165 cm^{-1} belongs to the B_{2g} mode of SnS [193-194].

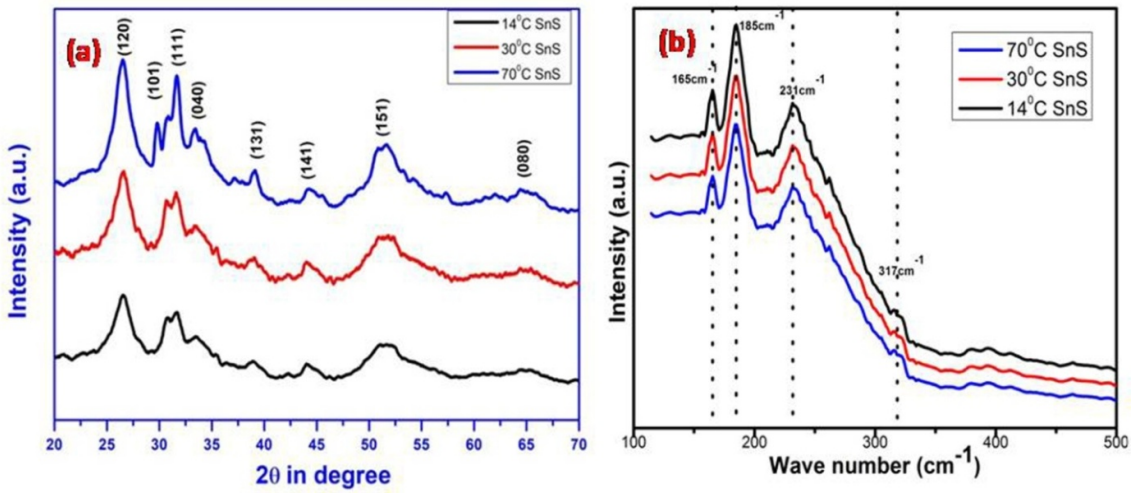

Fig. 3.16. (a) XRD pattern, (b) Raman spectra of as-prepared SnS growth in different temperatures

3.3.2.2. Morphological study

Morphology, crystal structure and particle size can be determined from Transmission Electron Microscopy (TEM) and High Resolution Transmission Electron Microscopy (HRTEM) analysis. TEM image (inset SAED) as well as HRTEM pattern of 14^0C SnS, 30^0C SnS and 70^0C SnS are shown in fig. 3.17(a,b,c) and fig. 3.17(d,e,f) respectively. From the HRTEM image it is confirmed that with increase of temperature the grain size increase. With increasing reaction temperature the kinetics mechanism of the particles increases. As a result there will be a tendency to agglomerate with each other. Hence, the kinetics of grain growth of the SnS nanocrystals is due to the increase in degree of abnormality with increasing temperature [196]. TEM image reveals that the particles are in almost spherical shape with average grain size of 5.02 nm at 14^0C, 8.16 nm at 30^0C and 10.26 nm at 70^0C SnS. Interplaner spacing of the individual crystals has been measured using image-J tools. The calculated lattice spacing of each sample is 0.29 nm for (101), 0.34 nm for (120) and 0.28 nm for (111) of 14^0C SnS, 30^0C SnS and 70^0C SnS respectively. Lattice fringes of all samples are displayed in the figures signifying crystallinity of grown SnS nanocrystals. From selected area electron diffraction (SAED) pattern it is clear that with increase in grain size the diffraction spot increases indicating increase in crystalline behavior.

Surface morphology and shape of the surface particles of as prepared samples have been characterized by FESEM analysis. Fig. 3.17(g,h,i) shows the FESEM images of 14^0C SnS, 30^0C SnS and 70^0C SnS respectively. Surface particles are spherical in shape. The size of the surface particles are less for 14^0C SnS whereas for 70^0C SnS it is large which tally with HRTEM results.

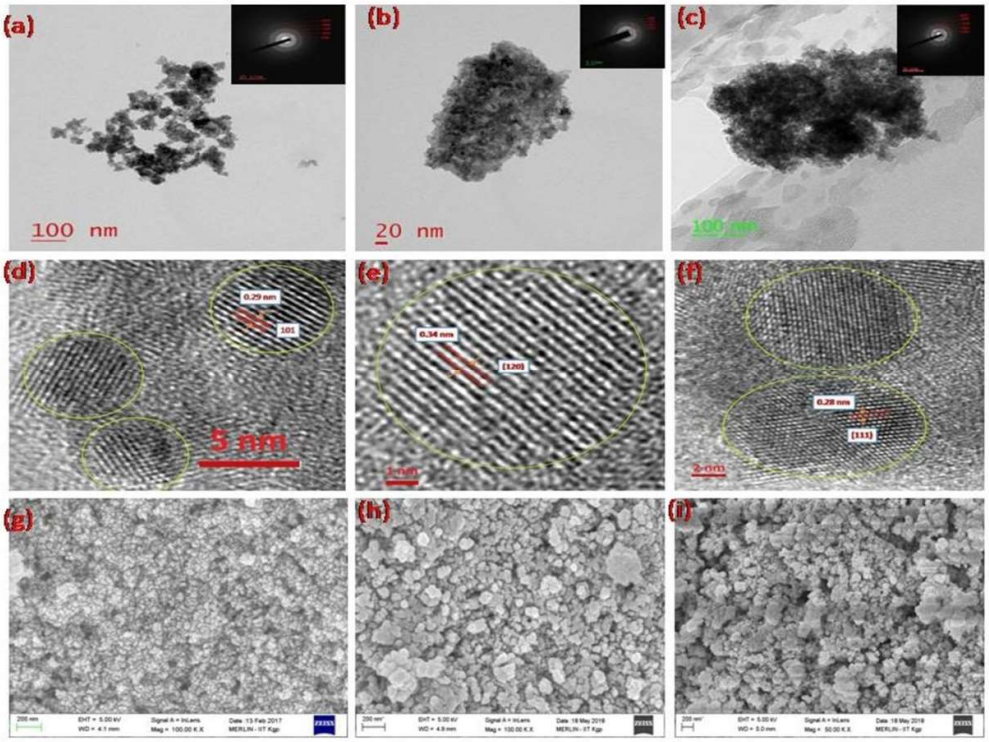

Fig. 3.17. TEM image and SAED (inset) pattern of (a)14 °C SnS (b) 30 °C SnS (c) 70 °C SnS, HRTEM image of (d) 14 °C SnS (e) 30 °C SnS (f) 70 °C SnS, FESEM image of (g) 14 °C SnS (h)30 °C SnS (i) 70 °C SnS

3.3.2.3. AFM analysis

Surface roughness of samples as prepared with variation of temperature i.e for 14^0C SnS, 30^0C SnS and 70^0C SnS were carried out by Atomic Force Microscopy (AFM) analysis.

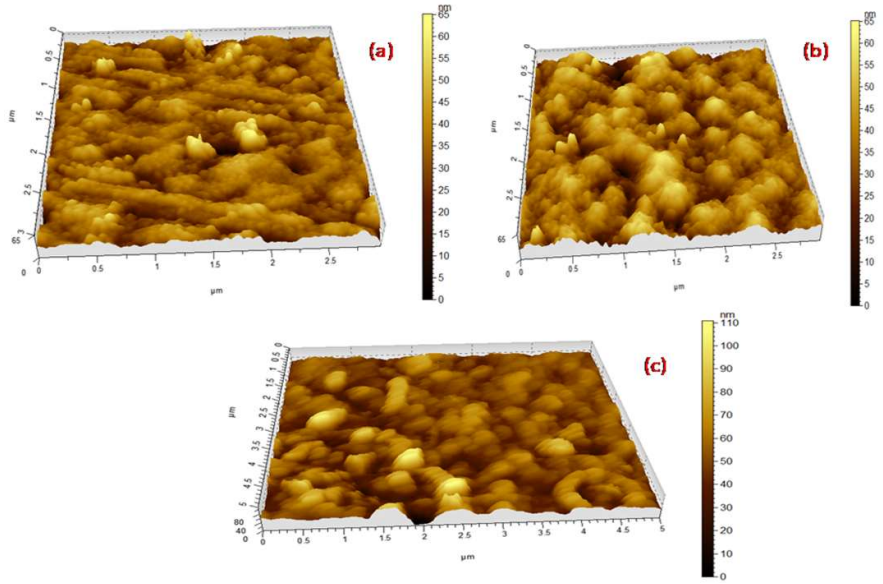

Fig. 3.18. 3-D AFM image of (a) 14 °C SnS (b) 30 °C SnS (c) 70 °C SnS

The samples are dispersed in ethanol and deposited on glass as film for AFM 3-D images and these are shown in fig. 3.18. The surface roughness of the 14 ^{0}C SnS, 30 ^{0}C SnS and 70 ^{0}C samples were 6.87 nm, 8.78 nm, and 11.4 nm respectively. With increase in growth temperature the surface roughnesses of the samples increase.

3.3.2.4. Composition analysis

Elemental compositions, percentage of atomic weight and clarity of as-prepared samples were confirmed by electron diffraction X-ray analysis (EDX). Fig. 3.19 gives the information about the compositional constituent of the said samples. EDX analysis shows that with increase in crystal size there is insufficiency in S whereas enhance in Sn content. Also it is seen that there are no impurities in EDX spectrum.

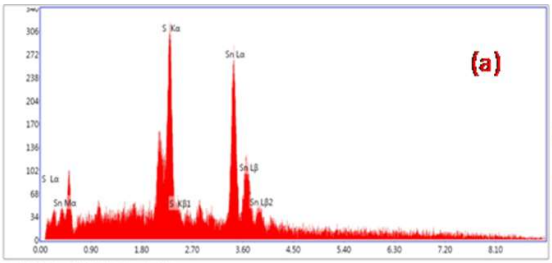

eZAF Smart Quant Results (b)

Element	Weight %	Atomic %	Net Int.	Error %	Kratio	Z	R	A	F
S K	24.46	54.52	563.77	6.63	0.29	1.31	0.89	0.89	1.02
Sn L	75.54	45.48	404.31	9.48	0.68	0.9	1.05	0.99	1.02

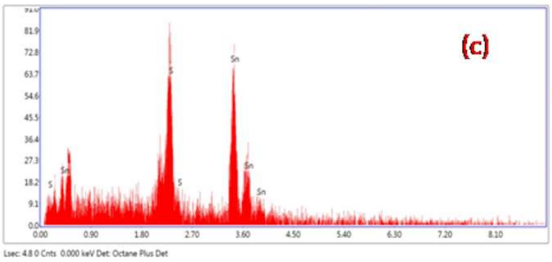

eZAF Smart Quant Results (d)

Element	Weight %	Atomic %	Net Int.	Error %	Kratio	Z	R	A	F
S K	23.50	53.21	364.18	8.52	0.28	1.31	0.88	0.89	1.02
Sn L	76.50	46.79	276.38	13.95	0.69	0.9	1.05	0.99	1.02

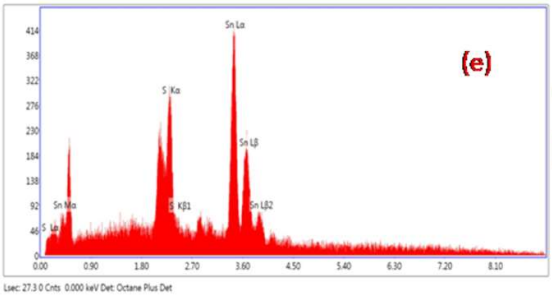

eZAF Smart Quant Results (f)

Element	Weight %	Atomic %	Net Int.	Error %	Kratio	Z	R	A	F
S K	17.91	44.68	272.13	6.63	0.22	1.34	0.87	0.88	1.02
Sn L	82.09	55.32	293.82	6.80	0.77	0.92	1.04	0.99	1.02

Fig. 3.19. EDAX pattern of (a) 14 °C SnS, (b) atomic ratio of Sn and S of 14 °C SnS; EDAX pattern of (c) 30 °C SnS, (d) atomic ratio of Sn and S of 30 °C SnS ; EDAX pattern of (e) 70 °C SnS, (f) atomic ratio of Sn and S of 70 °C SnS.

3.3.2.5. UV–Vis absorption spectroscopy study

To investigate the band structure of solid powder semiconducting materials UV-Vis spectroscopy study is an important experiment. Fig. 3.20(a) shows the variation of optical absorption coefficient of the samples with the wavelength in the optical range 250 nm-900 nm. From the absorption spectrum it is evident that SnS nanocrystals are good absorbing materials for solar light. Band gap of these temperature dependence SnS samples were calculated. To determine the band gap of the nanocrystals the following relations have been used

$$(\alpha h\nu)^2 = C\,(h\nu - E_g) \qquad (3.3.1)$$ for direct band gap energy

$$\text{and } (\alpha h\nu)^{1/2} = C\,(h\nu - E_g) \qquad (3.3.2)$$ for indirect band gap energy

Where C is a constant, E_g is the band gap energy of the semiconducting material and α is the absorption coefficient of the samples.

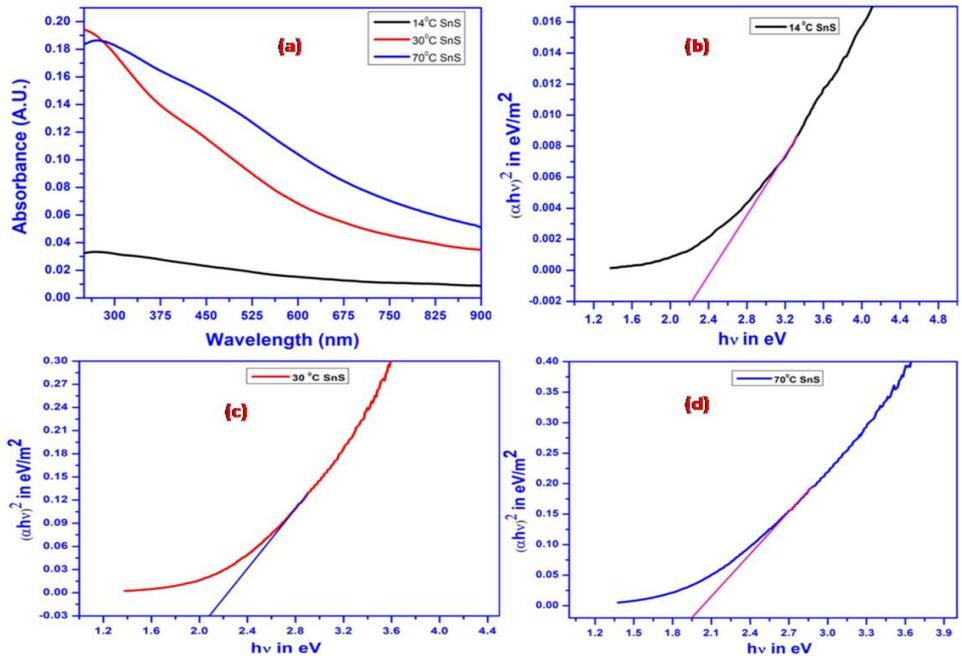

Fig. 3.20. (a) UV–Vis spectra of SnS in different growth temperatures. Band gap determination graphs of (b) 14 °C SnS (c) 30 °C SnS (d) 70 °C SnS

A plot of $(\alpha h\nu)^2$ vs. photon energy (hν) of each samples is depicted in fig. 3.20(b,c,d). The variation of $(\alpha h\nu)^2$ vs. photon energy (hν) is a straight line. A tangent has been drawn on the

linear part of the straight line in $(\alpha h\nu)^2$ vs. photon energy ($h\nu$) curve. The intercepts on the photon energy ($h\nu$) axis i.e $(\alpha h\nu)^2 = 0$ gives the direct band gap of the samples. The experimentally measured band gap of the 14^0C SnS, 30^0C SnS and 70^0C samples were 2.22 eV, 2.08 eV and 1.95 eV respectively. From UV-VIS absorption spectroscopy study it is clear that with increase in growth temperature the band gap energy of the samples decrease. The decrease in band gap energy is due to the increase in particle size with growth temperature. With increasing reaction temperature the kinetics mechanism of the particles increases. As a result there will be a tendency to agglomerate with each other. Hence, the kinetics of grain growth of the SnS nanocrystals is due to the increase in degree of abnormality with increasing temperature [196].

3.3.2.6. Photoluminescence spectroscopy study

Room temperature PL spectra of as synthesized 14 ^{0}C SnS, 30 ^{0}C SnS and 70 ^{0}C is shown in fig. 3.21. PL emission peaks are obtained at 586.81 nm (2.11eV), 597.73 nm (2.07eV) and 671.23 nm (1.84eV) at an excitation wavelength 430 nm of 14 ^{0}C SnS, 30 ^{0}C SnS and 70 ^{0}C.

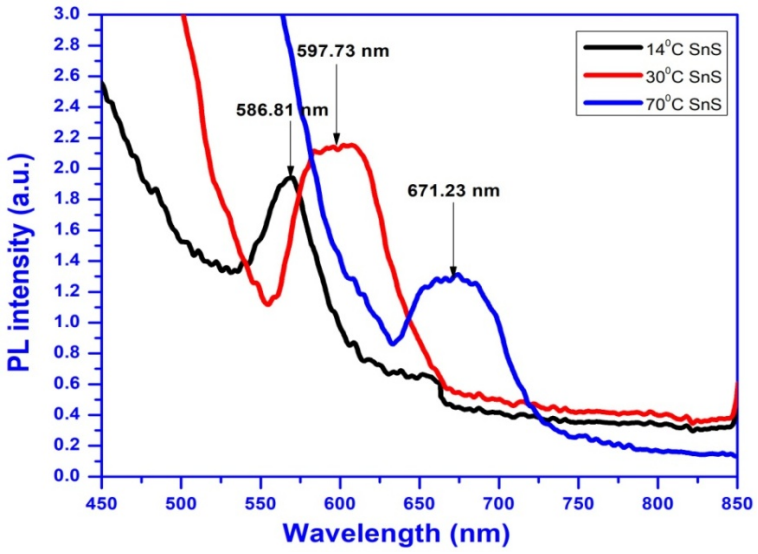

Fig. 3.21. Photoluminescence spectra of as-prepared SnS growth in different temperatures

It is clear from the PL spectra that with increase of growth temperature PL peaks are shifted towards higher wavelength region. This is probable due to the fact that with increase of growth temperature the size of the crystals increases. These peaks mainly arise from close to band edge due to the different surface states of sulfur vacancies [46]. These types of luminescence are the result of the recombination of exactions or shallowly electron-hole pairs [197].

3.3.2.7. Time-Correlated Single Photon Counting (TCSPC) study

One of the most beautiful experiments to determine PL decay life time of the carriers was carried out by Time-Correlated Single Photon Counting (TCSPC) measurement. Here a short flash laser source of wavelength 467 nm was used to excite the carriers of the samples. The carriers are excited to the higher energy state and then after a certain moment these carriers are coming back to the ground state. The PL decay life time of the carriers can be evaluated by the following working formula

$$\tau_{av} = \sum \frac{\alpha_i \tau_i}{\alpha_i} \qquad (3.3.3)$$

Where $\tau's$ are the decay components and α's are the respective amplitudes of life time components.

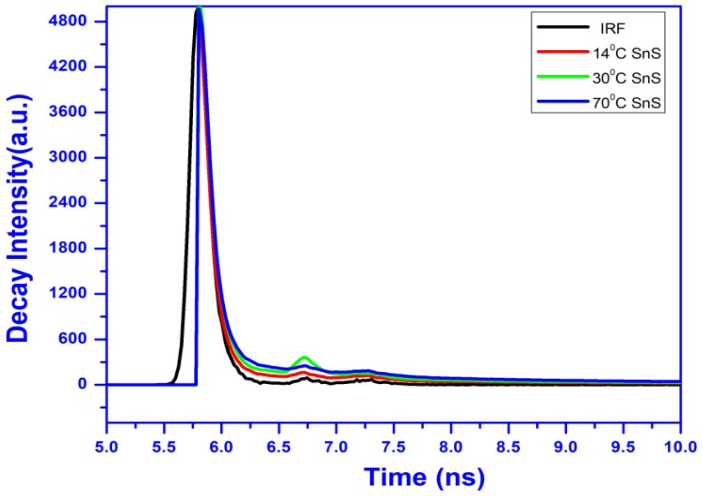

Fig. 3.22. TCSPC spectra of as-prepared SnS growth in different temperatures

The measured values of the carrier PL decay life time were 28.90 ps, 30.40 ps and 35.60 ps of 14^0C SnS, 30^0C SnS and 70^0C SnS respectively (fig. 3.22). From TCSPC (Time Correlated Single Photon Counting) measurements it is clear that with increase of growth temperature PL decay life time increases. The increase of PL decay life time is due to the increase in crystal size with increase in growth temperature [198].

Table: 3.3

Summarization table of result obtained from structural, morphology and optical characterization of SnS

Samples	Pattern	Crystal structure from XRD	Crystal size (nm) from HRTEM	Surface morphology from FESEM	Surface Roughness (nm)of SnS Nanofilm from AFM	Band gap (eV) from UV-VIS spectroscopy	PL peak (nm) position	PL decay life time (ps) from TCSPC
14^0C SnS	Particle	Orthormbic	5.02	Spherical	6.87	2.22	586.81	28.9
30^0C SnS	Particle	Orthormbic	8.16	Spherical	8.78	2.08	597.73	30.4
70^0C SnS	Particle	Orthormbic	10.26	Spherical	11.4	1.95	671.23	35.6

3.3.2.8. Electrical properties study

To fabricate optoelectronics device by new innovative materials it is very urgent to study the electrical properties of that materials. Fig. 3.23 shows the schematic diagram of hall measurement set up to study the electrical properties of SnS nanofilm. The variation of electrical conductivity with substrate temperature in the temperature range 300-345 K is depicted in fig. 3.24 (a). From the fig. 3.24 (a) it is clear that with increase in substrate temperature the conductivity of the SnS nanofilms ($14\ ^0$C SnS, $30\ ^0$C SnS and $70\ ^0$C SnS) increase which indicates the semiconducting behaviour of the nanocrystals. Grain size take

plays an important role for the variation of electrical conductivity with substrate temperature [199].

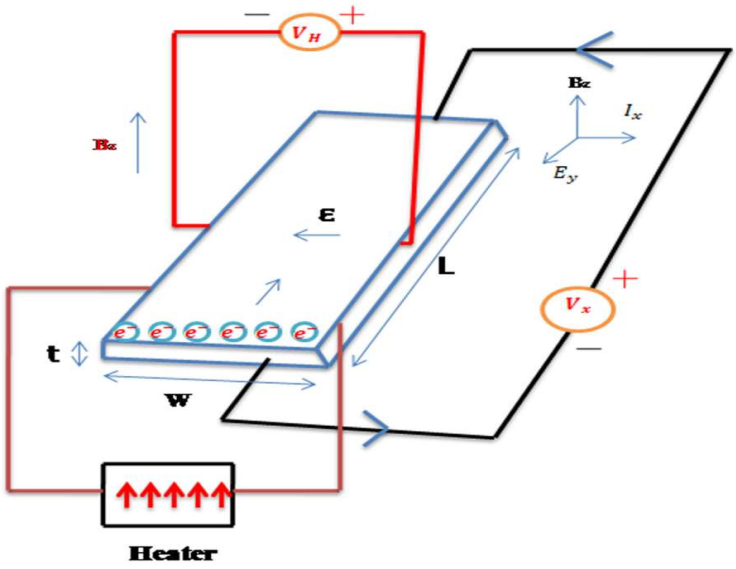

Fig. 3.23. Schematic diagram of hall measurement of SnS

Also smaller the crystal size higher is the resistivity. The room temperature (300K) conductivity of the 14 ^{0}C SnS, 30 ^{0}C SnS and 70 ^{0}C SnS nanofilm were 0.020 ohm^{-1} cm^{-1}, 0.025 ohm^{-1} cm^{-1} and 0.037 ohm^{-1} cm^{-1} respectively.

The activation energy of the SnS nanofilms was calculated from the Arrhenius equation

$$\sigma = \sigma_0 exp\left(-E_a/kT\right) \qquad (3.3.4)$$

where σ is the electrical conductivity of the SnS nanofilms, σ_0 is the pre-exponential factor, k is the Boltzmann constant and E_a is the activation energy of the SnS nanofilms. A plot ln σ versus 1/T is shown in fig. 3.24(b). Activation energies (E_a) of the SnS nanofilms were evaluated from the slop of the curve. 0.864 eV, 0.731 eV and 0.584 eV are the measured values of the activation energies of 14^{0}C SnS, 30^{0}C SnS and 70^{0}C SnS nanofilm respectively. It is very clear that with increase of growth temperature i.e. with increase of crystal size activation energy decrease. This is mainly due to the fact that with increase of crystal sizes

the surface to volume ratio decrease. The decrease in activation energy with increase in crystal size mainly depends on the surface barrier. For smaller crystal size greater is the surface barrier and hence greater is the activation energy. Fig. 3.24(c) gives the variation of carrier concentration with the substrate temperature in moderately low temperature region (300-345K). It is seen that carrier density increase with increase of substrate temperature. At room temperature the samples showed a carrier concentration about 10^{13} cm^{-3} and it reaches a maximum value in the order of 10^{15} cm^{-3} at 345 K. With increase of substrate temperature more and more number of electrons jumps to the conduction band and hence carrier concentration increases.

Considering the relation between hall mobility and drift mobility we have plotted the variation of drift mobility with substrate temperature of 14^0C SnS, 30^0C SnS and 70^0C SnS nanofilm (fig. 3.24 d) in the moderately low temperature (300-345 K). It is clear that with increase of substrate temperature the drift mobility decrease indicating that lattice scattering is predominant. In this moderately low temperature (300-345 K) drift mobility is found to be $\boldsymbol{\mu_D} \propto T^{-3/2}$. At room temperature the mobility of 70^0C SnS nanofilm is less than the 14^0C SnS nanofilm. To relate the relation among electrical conductivity ($\boldsymbol{\sigma}$), carrier concentration ($\boldsymbol{n}$) and drift mobility ($\boldsymbol{\mu_D}$),

$$\boldsymbol{\sigma = ne\mu_D} \qquad (\mathbf{3.3.5})$$

is the most useful fundamental equation. In case of 70^0C SnS the crystal size is more than the 14^0C SnS. The rate of increase in carrier concentration is greater than the rate of increase in conductivity with temperature for 70^0C SnS nanofilm. On the other hand, rate of increase in carrier concentration is less than the rate of increase in conductivity with temperature for 14^0C SnS nanofilm. The decrease in drift mobility of the charge carriers with increase of substrate temperature is due to the highly increase of carrier concentration [106]. The measured value of the drift mobility at room temperature (300 K) are ~ 920.670 cm^2/Vs,

~777.360 cm^2/Vs and ~755.350 cm^2/Vs of of 14 ^{0}C SnS, 30 ^{0}C SnS and 70 ^{0}C SnS nanofilm respectively. At 345 K it is found to be decreased to ~ 219.76 cm^2/Vs, ~202.10 cm^2/Vs and ~120.72 cm^2/Vs.

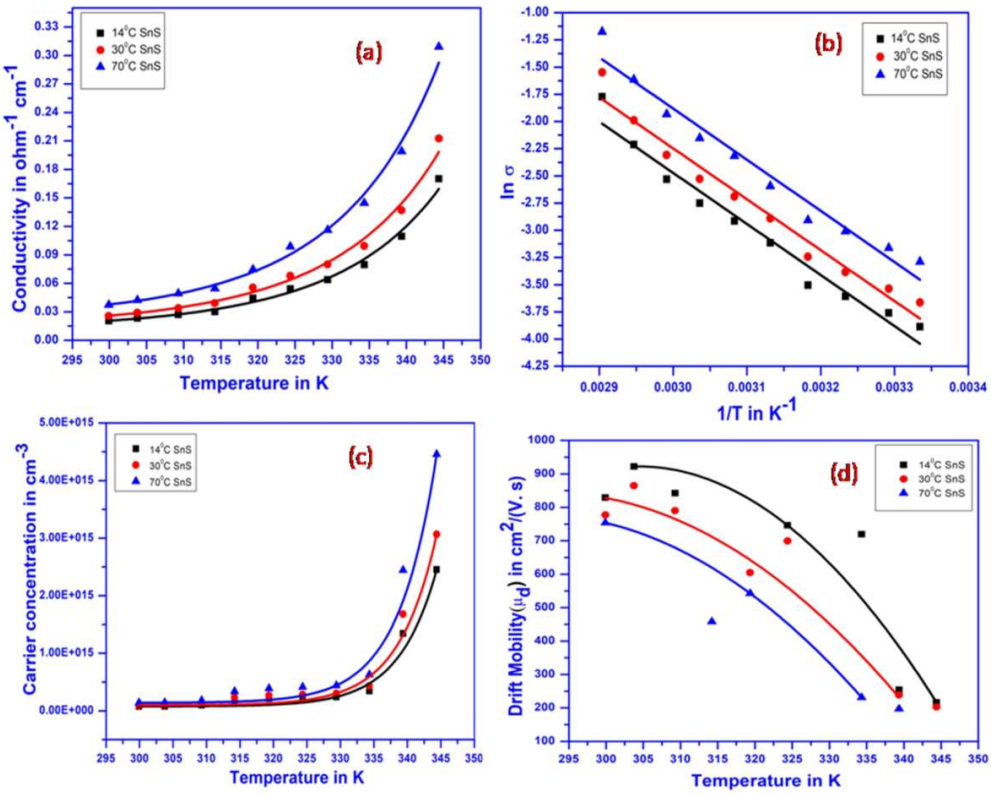

Fig. 3.24. (a) Electrical conductivity (σ) as a function of substrate temperature of SnS (b) Plot of $ln\sigma$ with 1/T of SnS (c) Variation carrier concentration with substrate temperature of SnS (d) Variation carrier drift mobility with substrate temperature of SnS

Table: 3.4

Electrical parameters from the Hall measurements of SnS nanofilms at room temperature

Physical Parameters	Measured Values		
	14^0 C SnS Nanofilm	**30^0 C SnS Nanofilm**	**70^0 C SnS Nanofilm**
Resistivity ρ (ohm-cm)	48.65	38.95	26.82
Conductivity σ (ohm^{-1} cm^{-1})	0.020	0.025	0.037
Activation energy E_a (eV)	0.864	0.731	0.584
Carrier concentration n (cm^{-3})	7.05×10^{13}	1.03×10^{14}	1.54×10^{14}
Drift Mobility μ_D (cm^2/Vs)	920.67	777.36	755.35
Hall coefficient R_H (cm^3 $coloumb^{-1}$) ($\mu_D \times \rho$)	44.79×10^3	30.27×10^3	20.25×10^3
Type of conductivity	p- type	p-type	p-type

3.3.3. Conclusion

SnS nanocrystals were synthesized by simple wet chemical precipitation method. XRD results shows that the crystals are orthorhombic in phase. TEM images indicate that the grain sizes are almost spherical within the range 5 nm to 10 nm. Crystalline nature of the sample was confirmed by HRTEM. Surface roughness was found to increase for samples with higher growth temperature. EDAX analysis shows that the samples have good stoichiometric ratio of Sn/S. From UV-VIS absorption spectra it is evident that SnS nanocrystals are good absorbing materials for visible light in the optical range 200 nm-900 nm. A decrease in band gap is observed as particle size increase with increase of growth temperature. PL spectra indicate a red shift of SnS nanocrystals occurred with increase growth temperature. The temperature variation of p- type SnS nanocrystals indicates electrical conductivities were ranging from 0.020 ohm^{-1} cm^{-1} to 0.037 ohm^{-1} cm^{-1} and carrier concentrations were 7.05×10^{13} cm^{-3} to 1.54×10^{14} cm^{-3}. Carriers drift mobilities were found to be high as 920.67 cm^2/Vs, 777.36 cm^2/Vs and 755.35 cm^2/Vs respectively. The decrease of mobility with temperature is due to the increase of concentration of defects in the grown

nanocrystals. In this moderately low temperature (300-345 K) drift mobility is found to be $\mu_D \propto T^{-3/2}$. With the increase of substrate temperature the drift mobility decrease indicating that lattice scattering is predominant. Therefore SnS nanocrystals have low resistivity, higher drift mobility, higher carrier concentrations, small PL decay life time and high absorption coefficient. Thus grown SnS nanocrystals exhibited excellent properties for the fabrication of optoelectronic devices.

3.4. Structural and Optical Characterization of SnS Nanoparticles Grown by Varying Reagent Ratio using Wet Chemical Precipitation Method

Here we have followed wet chemical precipitation method to grow SnS nanoparticle by varying reagent ratio of tin (II) chloride and sodium sulfide. We have maintained ratio of $SnCl_2.2H_2O$ and Na_2S. XH_2O are in 1:1, 1:3 and 1:5. The as prepared NPs are studied structurally and optically. The structural characterization of the samples was done using X-ray diffraction (XRD) and transmission electron microscopy (TEM). The chemical composition of the samples was confirmed by EDAX analysis. Optical characterizations were examined through optical absorption (UV-vis) and photoluminescence (PL) spectroscopy. From TEM image we see that the particle size is less (~ 3.22 nm) for SnS nanoparticles grown under 1:3 ratios. An increase in band gap is observed with increasing the ratio of Sn:S.

3.4.1. Experimental section

Tin sulfide (SnS) nanoparticles were synthesized through wet chemical precipitation method with the variation of reagent ratio. The molecular weight of $SnCl_2.2H_2O$ and $Na_2S.XH_2O$ were varied under the ratio of 1:1, 1:3 and 1:5. The $SnCl_2.2H_2O$ and $Na_2S.XH_2O$ was used as sources of tin and sulfur respectively. Deionized (DI) water was used as reaction medium. Triethanolamine (TEA) was employed as catalytic. Stirring was continued with a magnetic stirrer for 2 hours at room temperature at a constant speed. The obtained precipitates were centrifuged and washed with DI water for many times and dried at 40 ^{0}C for two days for characterization.

X-ray diffraction (XRD) data were recorded by Bruker Axs D2 phaser SSD160 with Cu-kα radiation (λ=1.5405Å) in the range of 20° to 70°. Transmission electron microscopy (TEM) was done by JEOL JEM200 operating at 200KV. The surface micrographs of the as prepared samples have been studied by FESEM using ZEISS MERLIN6105. Optical

absorption spectroscopies of the nanoparticles were analyzed by Shimadzu- Pharmaspec-1700 visible and ultraviolet spectrophotometer in the visible range at room temperature. The PL spectra of as prepared SnS were investigated by Perkin Elmer LS55 Fluorescence Spectrometer.

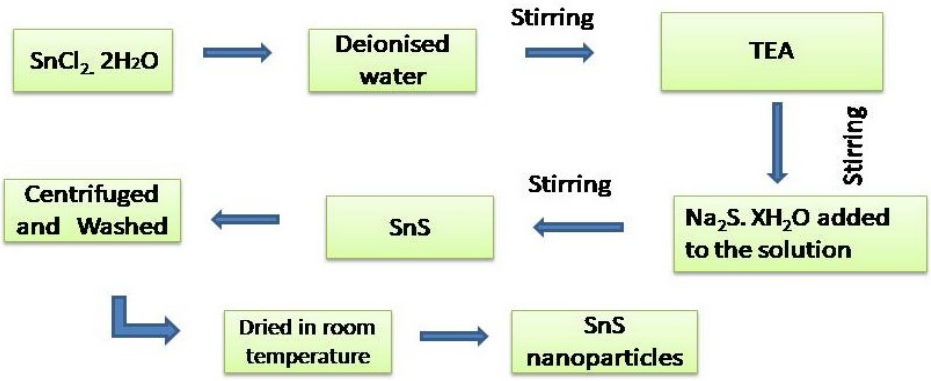

Fig. 3.25. Block diagram for sample preparation

3.4.2. Results and discussion

3.4.2.1. Structural analysis by X-ray diffraction (XRD)

The XRD pattern of the SnS nanoparticles grown under different reagent ratio (1:1, 1:3 and 1:5) is depicted in the fig. 3.26. The diffraction pattern has been taken in the range of 2θ value from 20^0 to 70^0.

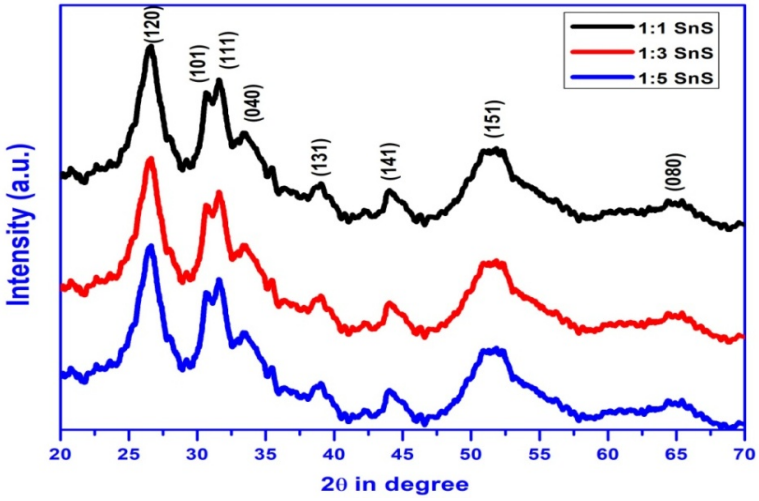

Fig. 3.26. XRD image of SnS nanoparticles under different reagent ratio

All the diffraction planes are clearly identified and perfectly matched with orthorhombic crystal structure of SnS as comparing with JCPDS data. (JCPDS card no: 39-0354). The broadening of the diffraction peaks indicates the formation of SnS nanoparticles. From the diffraction pattern it is confirmed that with the increase of regent ratio the half width of the diffraction peak increases which indicates the decrease in the crystal size.

3.4.2.2. Morphological analysis by TEM and FESEM

Morphological properties i.e the transmission electron microscopic (TEM) image as well as SADE pattern (inset) of the synthesized products under different amount of chemical reagent are shown fig. 3.27 (a,b,c). The crystal diameter of the prepared NPs was found to be varied from 3 nm to 8 nm. The TEM micrograph confirmed that with the increase of amount of Na_2S. XH_2O, the grain size decreases. The best smaller particle size of 3.22 nm was obtained for the SnS nanoparticles grown under reagent ratio of 1:3.

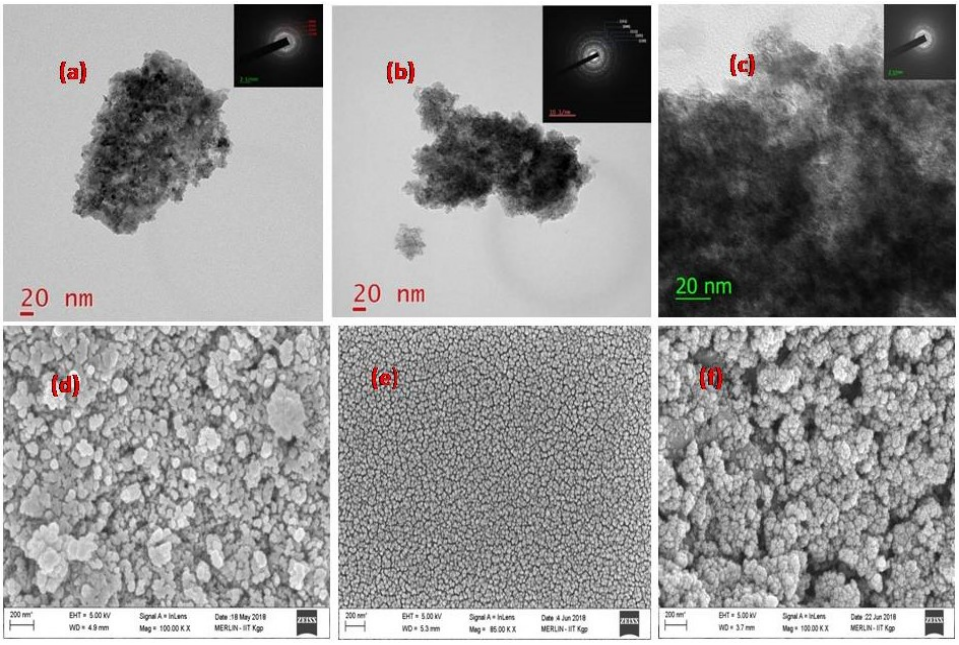

Fig. 3.27. TEM image and SAED (inset) pattern of (a) 1:1 SnS (b) 1:3 SnS (c) 1:5 SnS, FESEM image of (d) 1:1 SnS (e) 1:3 SnS (f) 1:5 SnS.

Surface micrograph, shape and size of the samples were analysed by FESEM. Fig.3.27 (d,e,f) depicted the FESEM image of the compositional varying SnS nanoparticles.

The surface particles are in particle nature. The beautiful surface micrograph was found for the 1:3 ratio varying sample. Therefore FESEM result tally with TEM result.

3.4.2.3. EDAX analysis

The EDAX spectrum of the prepared SnS product is shown in fig. 3.28(a) to 3.28(c). The reported results are depicted in table. It is found that with increase of reagent ratio of Sn/S, there is an increase of sulphur (S) content for all samples. The change in band gap energy is mainly due to quantum confinement effect.

1:1 SnS

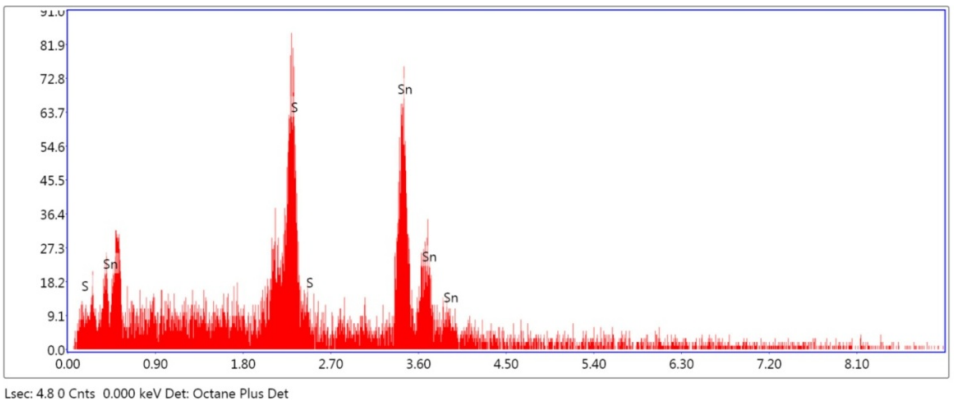

Fig. 3.28. (a) EDAX spectrum of SnS nanoparticles grown under the reagent ratio of 1:1

1:1 SnS

Element	Weight %	Atomic %	Net Int.	Error %	Kratio	Z	R	A	F
S K	23.50	53.21	364.18	8.52	0.28	1.31	0.88	0.89	1.02
SnL	76.50	46.79	276.38	13.95	0.69	0.9	1.05	0.99	1.02

1:3 SnS

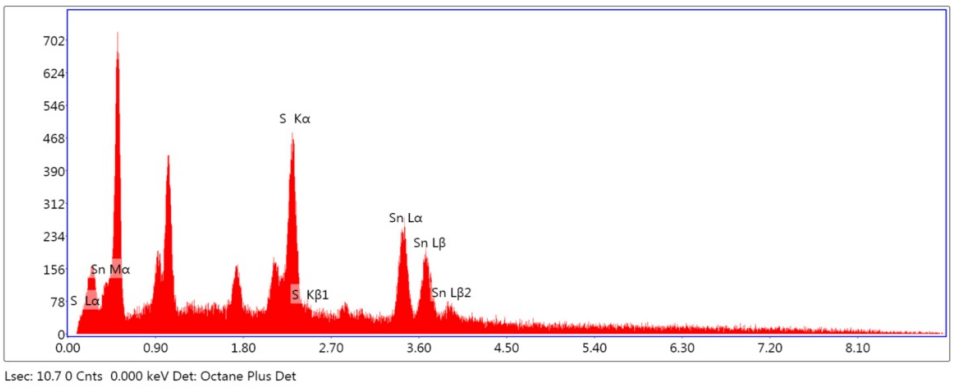

Fig. 3.28. (b) EDAX spectrum of SnS nanoparticles grown under the reagent ratio of 1:3

1:3 SnS

Element	Weight %	Atomic %	Net Int.	Error %	Kratio	Z	R	A	F
S K	31.09	62.54	731.86	5.49	0.36	1.27	0.9	0.9	1.02
SnL	68.91	37.46	371.63	9.51	0.60	0.88	1.06	0.99	1.02

1:5 SnS

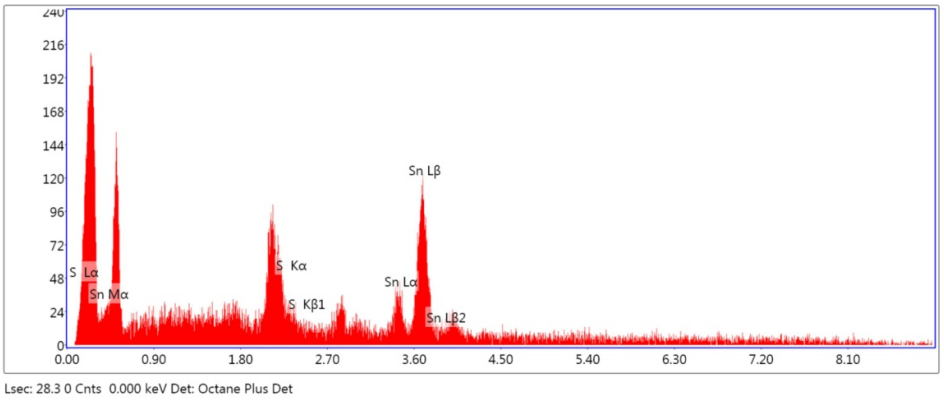

Fig. 3.28. (c) EDAX spectrum of SnS nanoparticles grown under the reagent ratio of 1:5

1:5 SnS

Element	Weight %	Atomic %	Net Int.	Error %	Kratio	Z	R	A	F
S K	36.40	67.93	50.26	9.36	0.42	1.25	0.91	0.91	1.02
SnL	63.60	32.07	19.90	12.97	0.54	0.86	1.07	0.98	1.02

3.4.2.4. Optical absorption study

The optical absorption study of the prepared product were analysed through UV-vis absorbance spectroscopy. The SnS nanoparticles were dispersed in ethanol for UV-vis absorption spectroscopic measurements.

The optical absorbance graph of prepared samples grown under different reagent ratio is presented in fig. 3.29 (a).

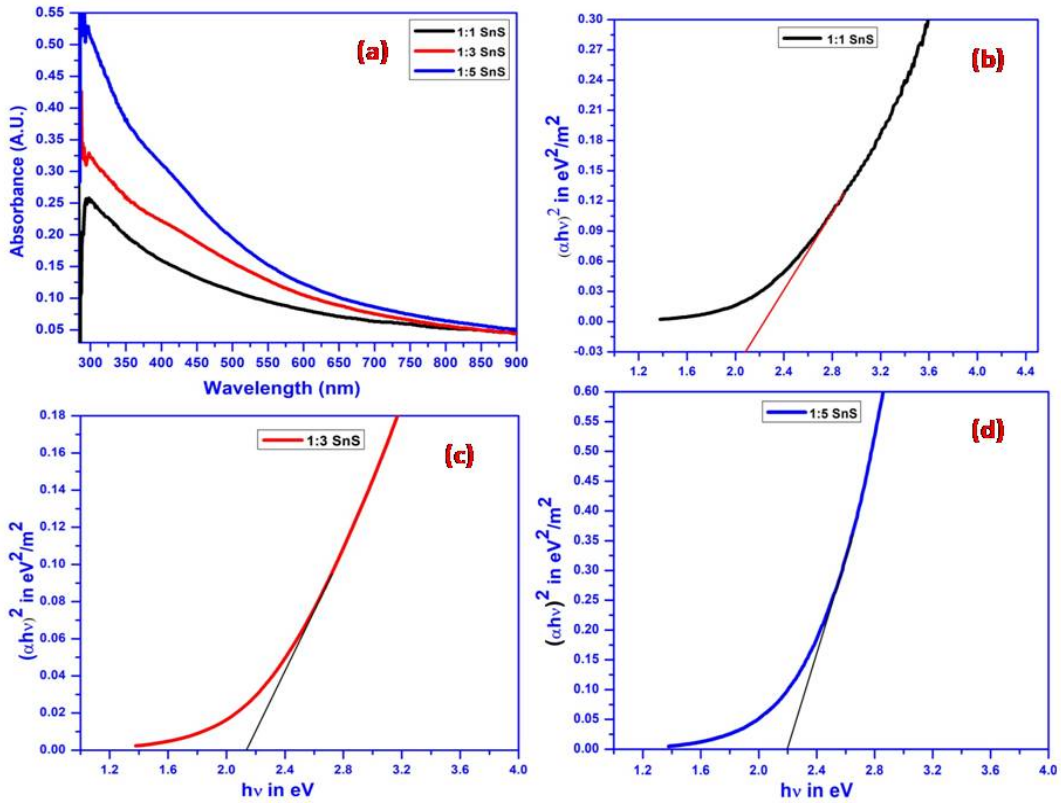

Fig. 3.29. (a) UV–Vis spectra of SnS nanoparticles under different reagent ratio; (b) Band gap determination graphs of (b) 1:1 SnS (c) 1:3 SnS (d) 1:5 SnS.

The data for absorption coefficient was taken in the optical range in between 300-900 nm. The plot of $(\alpha h\nu)^2$ vs. hν (fig. 3.29 b,c,d) was utilized to estimate the band gap energy of the samples. The band gap energy of the synthesized products was determined from the equation, $(\alpha h\nu) = C\,(h\nu - \Delta Eg)^{1/2}$, where C is a constant and ΔEg is the band gap energy of the sample. An increase in band gap was observed with the increase of atomic percentage of chemical

reagent. With the increase of reagent ratio the particle size decreases and this leads to increase in optical band gap energy [200]. Therefore the largest band gap energy of 2.20 eV was obtained for the 1:5 SnS sample.

3.4.2.5. Photoluminescence study

Photoluminescence (PL) study determines the impurity and defect level of materials. PL spectra (fig. 3.30) of the ratio varying samples were analysed at room temperature. From the PL spectra it is found that the emission peak position shifts towards the lower wavelength side.

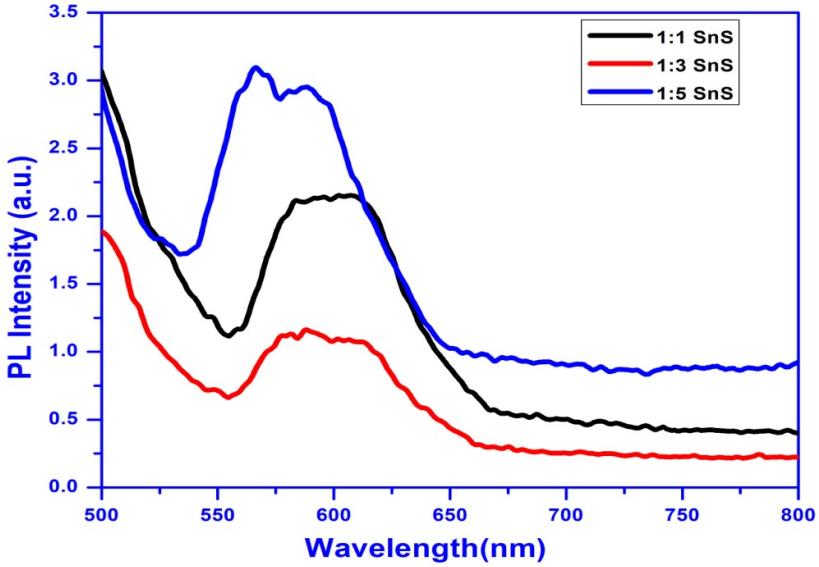

Fig. 3.30. PL spectra of as synthesized SnS nanoparticles grown at different reagent ratio

The decrease in particle size with the increase of reagent ratio, leads to increase in band gap energy [201]. Therefore, a blue shift is observed in PL spectra of SnS with increasing ratio of tin chloride and sodium sulfide. The PL peak position of 1:1 SnS, 1:3 SnS and 1:5 SnS sample arises at 597.93 nm, 582.10 nm and 566.33 nm respectively which are closer to the band gap energy of the SnS as measured from optical absorption graph. Hence, a band to band transition was observed in the all ratio varying samples.

Table 3.5

Summarization Table for structural and optical characterization

Samples	Pattern	Crystal structure from XRD	Crystal size (nm) from TEM	Surface morphology from FESEM	Atomic percentage from EDAX		Band gap (eV) from UV-VIS spectroscopy	PL peak (nm) position
					Sn	S		
1:1 SnS	Particle	Orthormbic	8.16	Spherical	46.79	53.21	2.08	597.73
1:3 SnS	Particle	Orthormbic	3.22	Spherical	37.46	62.54	2.13	582.10
1:5 SnS	Particle	Orthormbic	7.96	Spherical	32.07	67.93	2.20	566.33

3.4.3. Conclusion

The SnS nanoparticles have been prepared by cost effective wet chemical precipitation technique. The $SnCl_2.2H_2O$ and Na_2S. XH_2O was taken in the ratio of 1:1, 1:3 and 1:5. The XRD analysis confirmed the formation of SnS nanoparticles with orthorhombic crystal phase. The TEM image indicates that the crystal size decrease with the increase of chemical reagent ratio and the particle size 3.22 nm was found for 1:3 SnS sample. An excess of sulphur content was observed in EDAX spectrum for all sample. Optical band gap energy has been determined from optical absorption study. An increase in band gap (2.08 nm to 2.20nm) was observed with increasing the ratio of $SnCl_2$:Na_2S and it was found to be 2.20 nm for 1:5 SnS sample. PL spectra show that the peak position moved towards the lower wavelength region. Therefore, the chemical reagent ratio ($SnCl_2$:Na_2S) take place an important role on the structural as well as optical properties of SnS nanoparticles.

3.5. Synthesis and Characterization of Fe-doped SnS, Mn-doped SnS and pure SnS using Wet Chemical Precipitation Method

In the present work, we have successfully synthesized pure SnS, Fe-doped SnS and Mn-doped SnS by wet chemical precipitation technique. The as grown samples were characterized structurally by X-ray diffraction (XRD), Transmission electron microscopy (TEM) and Field emission scanning electron microscopy (FESEM). Purity of the samples was confirmed by EDAX study. The doping effect changes the crystal size of the SnS NPs. The highest particle size of ~6.80 nm was observed for Mn-doped SnS which is confirmed by TEM micrograph. Optical properties were studied by UV-VIS absorption spectroscopy, photoluminescence (PL) and time correlated single photon counting (TCSPC). Among the three samples Mn doped SnS shows lowest band gap energy of 2.00 eV.

3.5.1. Experimental section

Chemical precipitation technique was followed to grow Fe-doped SnS and Mn-doped SnS nanoparticles at room temperature. In this typical process, 1.125 gm of $SnCl_2.2H_2O$ was dissolved in 50 ml deionized water. Then 5 ml triethylamine (TEA) was added to the tin chloride solution under stirring condition. After that 40 ml (1.17 gm of $Na_2S.XH_2O$ in 40ml deionised water) sodium sulfide solution added drop wise (1:3 ratio) into the tin chloride solution followed by 0.01 mol (0.040 gm) of $FeCl_3$ and 0.01 mol (0.049 gm) of $MnCl_2.4H_2O$ solution respectively. Stirring were continued for 2 hours at room temperature. The products were centrifuged and washed with deionized water for many times and dried at 40^0C to obtain Fe-doped and Mn-doped SnS NPs. Undoped SnS was synthesized in same condition and similar process without mixing of $Fecl_3$ and $Mncl_2.4H_2O$ solution.

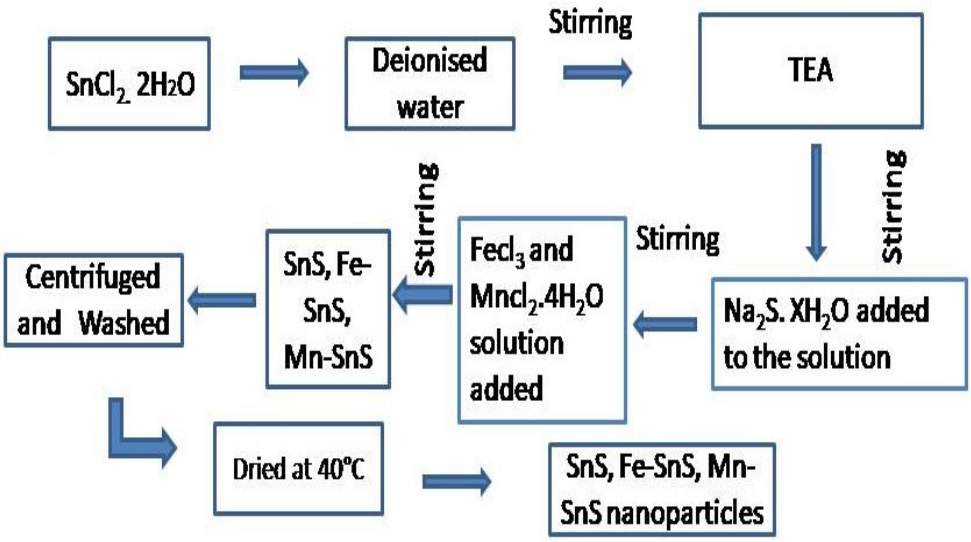

Fig. 3.31. Block diagram for synthesis process

X-ray diffraction (XRD) measurements of the samples were carried out by Bruker Axs D2 phaser SSD160 with Cu-kα radiation (λ=1.5405Å) ranging from 20° to 70°. Transmission electron micro-graph of the prepared samples was measured by JEOL JEM200 operating at 200KV. The surface morphology of as prepared samples has been characterized by FESEM using ZEISS MERLIN6105. Optical absorption spectra of samples were carried out in the wavelength range 200 nm-900 nm by Shimadzu- Pharmaspec-1700 visible and ultraviolet spectrophotometer. PL spectra of as prepared SnS, Fe doped SnS and Mn doped SnS NPs were taken by Perkin Elmer LS55 Fluorescence Spectrometer. Time-Correlated Single Photon Counting (TCSPC) of the pure SnS and doped SnS samples were studied by Delta flex-01-DD.

3.5.2. Results and discussion

3.5.2.1. XRD analysis

Fig. 3.32 shows the XRD results of as synthesized pure SnS, Fe doped SnS and Mn doped SnS. XRD data has been recorded through X-ray diffractometer by Bruker Axs D2 phaser SSD160 with Cu-kα line (λ=1.5405Å) in the range of 20° to 70°. In the XRD figure, peaks at 2θ of 26.42 (120), 30.56 (101), 31.50 (111), 33.32 (040), 39.09 (131), 44.03 (141),

64.31 (125) were recognized to orthorhombic of SnS. So these diffraction peaks are mainly comes from the orthorhombic crystal phase of SnS (JCPDS card no: 39-0354). The strong, sharp and well defined XRD peaks indicate that as prepared samples are crystallized in nature. Debye Scherer formula were used to calculate the approximate particle diameter

$$P = \frac{0.9\lambda}{\beta\cos(\theta)} \qquad (3.5.1)$$

Where, λ is the wavelength of incident X-rays (1.5405Å), $\beta_{1/2}$ is the full width half maximum Intensity (FWHM), θ is the Bragg angle, P is the average diameter of the particles. According to Debye Scherer formula, the estimated grain size of pure SnS, Fe doped SnS as well as Mn doped SnS were close to 2.06 nm, 2.36 nm and 2.66 nm respectively. There is no phase change occurring due to doping of Fe and Mn in SnS. Even their no extra peaks appear. This clearly shows that in the process of doping of SnS the dopant Fe^{3+} and mn^{2+} replaces the cation Sn^{2+}[202].

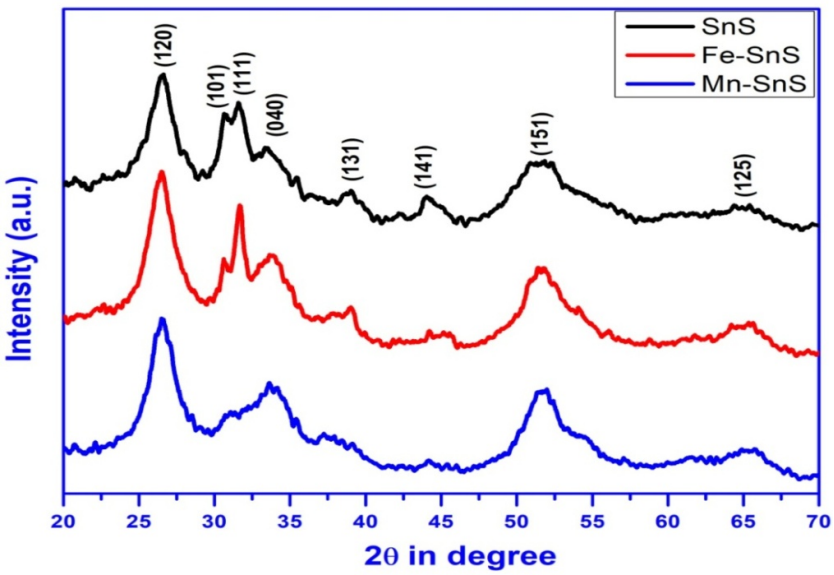

Fig. 3.32. XRD pattern of pure SnS, Fe doped-SnS and Mn-doped SnS

3.5.2.2. TEM and FESEM study

Morphology, shape of crystal and crystal size of pure SnS, Fe-doped SnS and Mn-doped SnS were determined from the Transmission Electron Microscopy (TEM) study. TEM

images (inset SAED) of pure SnS and doped SnS is presented in fig. 3.33(a,b,c). Image-J tools were used to determine the average grain sizes of pure SnS and doped SnS. From TEM study, it is clear that crystal size increase due to doping. It is seen that the particle sizes are maximum for Mn doped SnS whereas less for pure SnS. This increase in the particle size mainly depends on the electro negativity of the dopent [203]. The particle size lies in between 3 nm to 7 nm. Selected area electron diffraction (SAED) pattern confirmed the crystalline behaviour of SnS.

Field Emission Scanning Electron Microscopy (FESEM) study gives the idea about the shape and size of the surface crystals. Fig. 3.33(d,e,f) gives the FESEM picture of pure SnS as well as doped SnS. From FESEM analysis it is clear that the surfaces micrograph of the grown samples is in particle in nature and the crystal size is large for Mn doped SnS NPs.

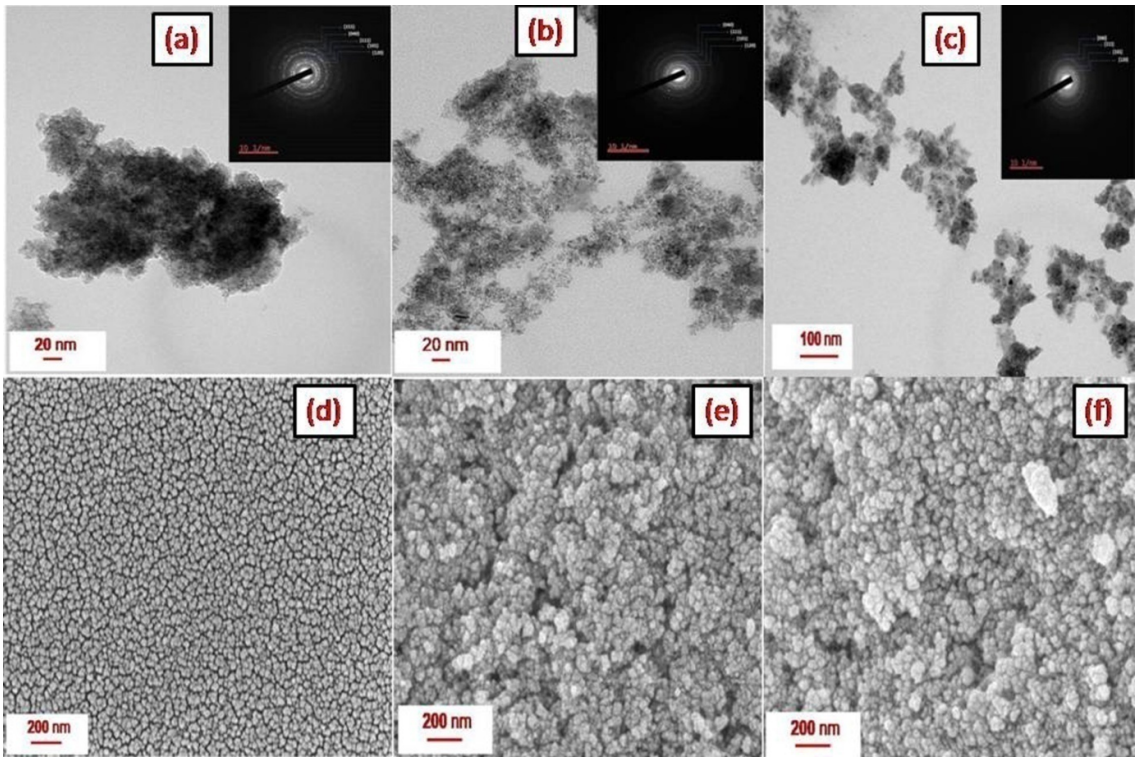

Fig. 3.33. TEM image and SAED (inset) pattern of (a) pure SnS (b) Fe doped SnS (c) Mn doped SnS; FESEM image of (d) pure SnS (e) Fe doped SnS (f) Mn doped SnS

3.5.2.3. EDAX study

Electron Dispersion X-ray Analysis (EDAX) mainly gives the information about the elemental percentage as well as purity of the said samples. EDAX spectrum and the corresponding atomic percentage of the pure SnS and the doped SnS are described in fig. 3.34 (a,b,c,d,e,f). EDAX result suggest that the dopant Fe^{3+} and mn^{2+} substitutes the Sn^{2+} cation on the basis of their atomic radius (atomic radius of Sn^{2+} , Fe^{3+} and Mn^{2+} are 0.93 Å, 0.63Å and 0.8Å respectively). It is clear that there is no impurity peak in the EDAX spectrum indicating the samples are in pure form.

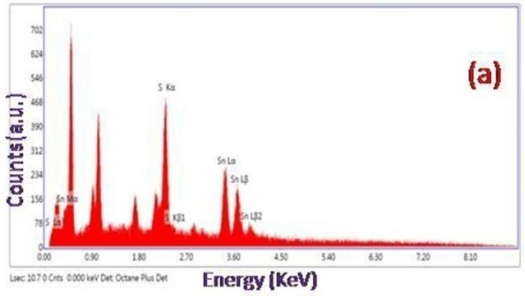

(d)

Elemen t	Weight %	Atomic %	Net Int.	Error %	Kratio	Z	R	A	F
S K	31.09	62.54	731.86	5.49	0.36	1.27	0.9	0.9	1.02
Sn L	68.91	37.46	371.63	9.51	0.60	0.88	1.06	0.99	1.02

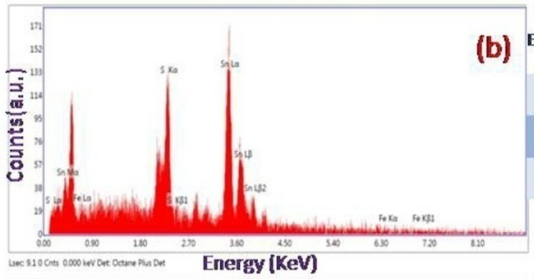

(e)

Elemen t	Weight %	Atomic %	Net Int.	Error %	Kratio	Z	R	A	F
Fe L	0.07	0.10	0.33	57.69	0.00	1.13	0.91	0.48	1
S K	18.24	45.20	328.50	9.22	0.22	1.34	0.87	0.88	1.02
Sn L	81.70	54.70	346.45	10.07	0.76	0.92	1.04	0.99	1.02

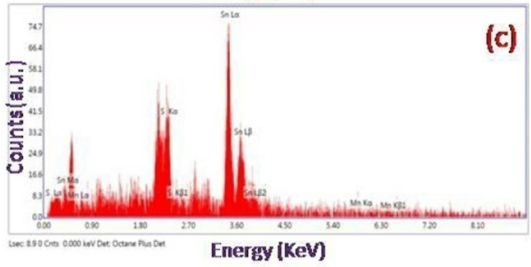

(f)

Elemen t	Weight %	Atomic %	Net Int.	Error %	Kratio	Z	R	A	F
S K	16.72	39.42	145.02	10.73	0.20	1.32	0.88	0.88	1.02
Sn L	73.07	46.53	149.50	12.81	0.67	0.91	1.05	1	1.02
Mn K	10.21	14.05	9.91	62.92	0.12	1.15	0.97	0.96	1.03

Fig. 3.34. EDAX spectrum of (a) pure SnS (b) Fe doped SnS (c) Mn doped SnS; Elemental percentages of (d) pure SnS (e) Fe doped SnS (f) Mn doped SnS.

3.5.2.4. Optical absorption (UV-vis) study

Optical absorption study mainly gives the information about the optical properties and the optical band gap of the semiconducting materials. Optical measurements of pure SnS, Fe

doped SnS and Mn doped SnS are taken in the optical range 230 nm to 900 nm. Fig. 3.35(a) shows the variation of optical absorbance coefficient with the wavelength of incident photon. The relation between the optical absorption coefficient (α) and the incident photon energy (hν) for the direct band gap semiconductors can be written as

$$(\alpha h\nu)^2 = C\,(h\nu - E_g) \qquad (3.5.1)$$

Where C is a constant, E_g is the optical band gap energy of the material and α is the optical absorption coefficient of the materials. The calculated direct band gap energy of the orthorhombic phase of pure SnS, Fe doped SnS and Mn doped SnS have been estimated from the intercepts of the plot $(\alpha h\nu)^2$ vs. hν are 2.13 eV, 2.09 eV and 2.00 eV respectively. The plot of $(\alpha h\nu)^2$ vs. hν of the samples are shown in fig. 3.35(b,c,d). Due to doping of transition metal there are obviously decrease in band gap energy. Among them, largest band gap reduction (~0.13 eV reduction) is observed in Mn doped SnS NPs. This reduction of band gap energy is mainly due to the electro negativity of transition metal ions and the lattice distortion influenced by doping together [204].

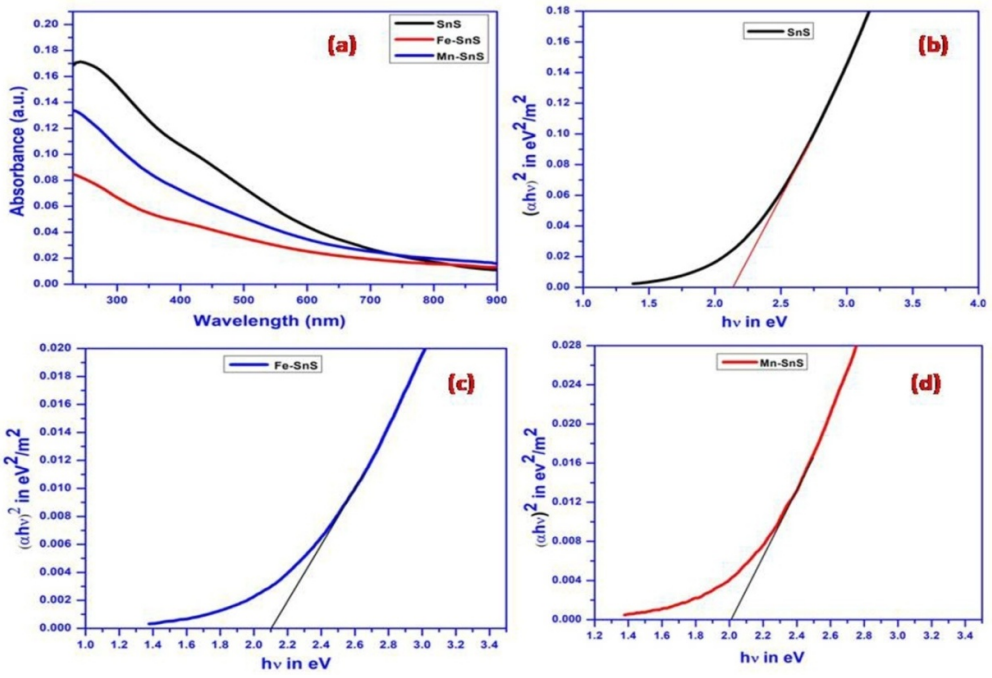

Fig. 3.35. (a) UV-VIS absorption spectra of as prepared samples; Plot of $(\alpha h\nu)^2$ vs. hν of (b) pure SnS (c) Fe doped SnS (d) Mn doped SnS.

3.5.2.5. Photoluminescence study

Photoluminescence spectroscopy (PL) is an important measurement to study the optical response as well as impurity state /defect state of the nanoparticles. A graph of the PL spectra of pure SnS, Fe doped SnS and Mn doped SnS are depicted in fig. 3.36. From the photoluminescence study it is clear that, PL peak shifted in the higher wavelength region for Mn doped SnS compared to the Fe doped and undoped SnS nanoparticles. The increase in particle size for Mn doped SnS leads to red shift in PL spectra of Mn-SnS NPs than the pure SnS and Fe-SnS NPs. Here we have used an excitation of wavelength 440 nm. The PL peaks of pure SnS, Fe doped SnS and Mn doped SnS are obtained at 589.03 nm (2.11 eV), 596.88 nm (2.07 eV) and 625.62 nm (1.98 eV) respectively. These emission peaks are probably attributed from close to the conduction band due to the defect states of sulfur vacancies and tin ion vacancies [205].

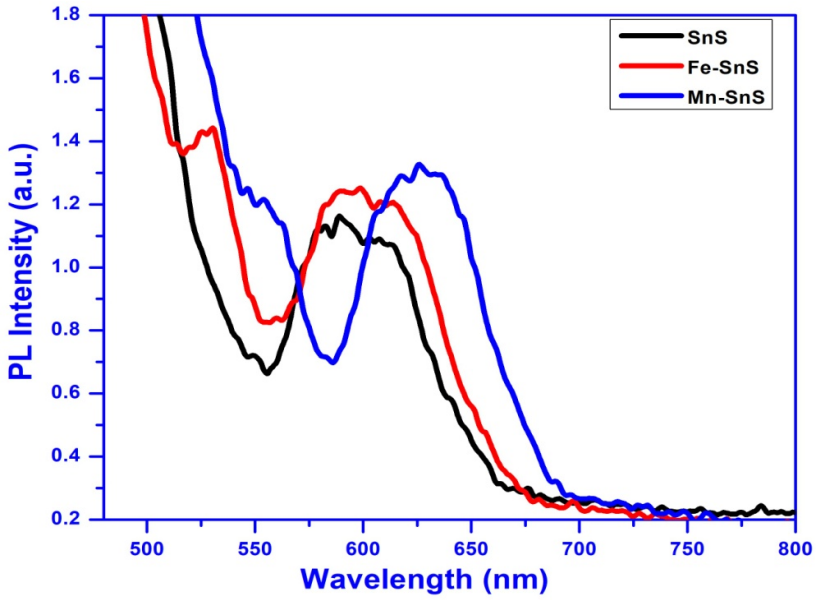

Fig. 3.36. Photoluminescence spectra of the samples

3.5.2.6. TCSPC analysis

Time-Correlated Single Photon Counting (TCSPC) measurement is used to study PL decay life time of materials. A laser source of incident wavelength 467 nm was used to excite

the carriers. With the incident radiation the carriers of the samples excited to the higher energy state and after a sometimes the carriers are returned to the ground state. The average PL decay life time of the carriers of the samples can be determined by the following formula

$$\tau_{av} = \sum \frac{\lambda_i \tau_i}{\lambda_i} \qquad (3.5.2)$$

Where, $\tau's$ are the decay components and λ's are the respective amplitudes of life time components. Fig. 3.37 shows the TCSPC spectra of as prepared samples. The calculated values of the carrier PL decay life time of pure SnS, Fe doped SnS and Mn doped SnS were 22.8 ps, 33.9 ps and 34.4 ps respectively. From TCSPC measurements it is evident that with increase of particle size, the PL decay life time increases. The increase in PL decay life time is due to the fact that with increase in crystal size the surface states are minimized. The experimental results of structural, morphology and optical characterization of the samples are defined in table 3.6.

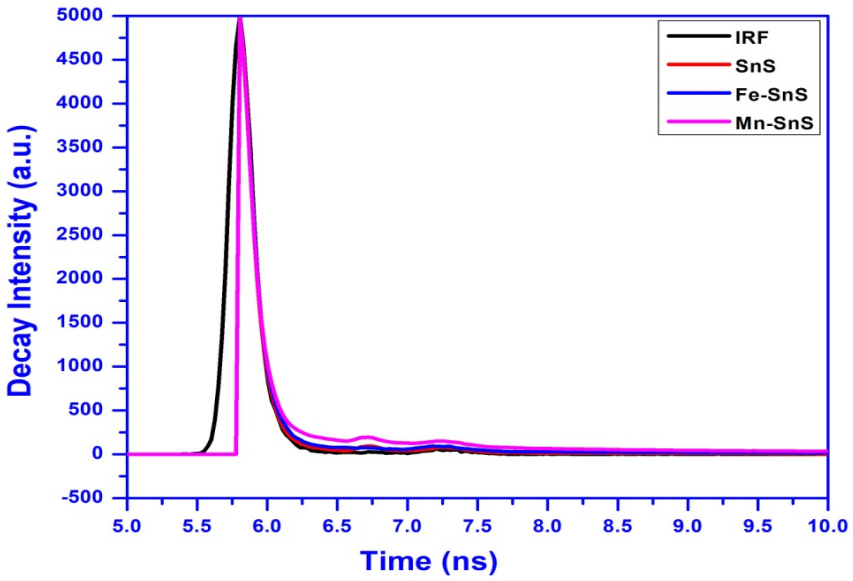

Fig. 3.37. TCSPC spectra of the as prepared samples

Table: 3.6

Structural and optical parameters of the prepared pure SnS and doped SnS NPs

Samples	Pattern	Crystal structure from XRD	Crystal size (nm) from TEM	Surface morphology from FESEM	Band gap (eV) from UV-VIS spectroscopy	PL peak (nm) position	PL decay life time (ps) from TCSPC
Pure SnS	Particle	Orthormbic	3.22	Spherical	2.13	582.1	22.8
Fe-doped SnS	Particle	Orthormbic	5.22	Spherical	2.09	593.3	33.9
Mn-doped SnS	Particle	Orthormbic	6.80	Spherical	2.00	620.0	34.4

3.5.3. Conclusion

Pure SnS, Fe doped SnS and Mn doped SnS were prepared by simple chemical precipitation method. XRD results indicate the orthorhombic crystal phase of the prepared SnS samples. Diffraction pattern also confirmed that the dopant Fe^{3+} and mn^{2+} replaces the cation Sn^{2+} in SnS host without changing its structural phase. TEM results show the crystal size increase due to doping and the grain size is greater for Mn doped SnS NPs. The crystal sizes are varied from 3 nm to 7 nm. This increase in crystal size of the doped NPs is mainly depends on the electronegativity of the dopent elements. EDAX analysis confirmed that doping elements are present in the doped SnS. No impurity peaks in the EDAX spectrum are observed signifying the prepared samples are in pure form. Largest band gap reduction (~0.13 eV reduction) is observed in Mn doped SnS compared to pure as well as Fe doped SnS. This reduction of band gap energy is due to the electronegativity of transition metal ions and the lattice distortion influenced by doping together. The PL study shows that the emission peak of Mn doped SnS shifted towards the higher wavelength side which is due to the increase in particle size.

3.6. Synthesis and Characterization of SnS and SnS-Ag Nanocomposites by Solvothermal Method

SnS and SnS-Ag nanocomposite were synthesized by cost effective solvothermal technique. Structural properties were characterized by X-ray diffraction (XRD), Transmission Electron Microscopy (TEM) and Field Emission Scanning Electron Microscopy (FESEM). Elemental compositions were confirmed by Electron Diffraction X-ray Analysis (EDAX). The Optical properties were characterized by UV-VIS absorption spectra, Photoluminescence spectra (PL) and Time Correlated Single Photon Counting (TCSPC). XRD results suggest that the samples are in orthorhombic structure in phase. TEM results indicate that quantum dot like particles (5 nm to 8 nm) are observed in both SnS and SnS-Ag nanostructures. The crystalline nature of the samples was confirmed by SAED. EDAX analysis confirmed that Ag is present in SnS-Ag nanocomposite. From optical absorption study it is clear that SnS-Ag nanocomposite is a good absorber in the sun light than SnS nanocrystal. A decrease in the band gap of SnS-Ag nanocomposite was observed compared to SnS. The PL study indicates that a peak shift of SnS-Ag naocomposite was observed towards the higher wavelength side.

3.6.1. Experimental section

Tin sulfide nanoparticles (SnS) were prepared by solvothermal method. For this purpose 1.13 gm tin chloride ($SnCl_2.2H_2O$) and 0.39 gm sodium sulfide ($Na_2S{\cdot}XH_2O$) were dissolved individually in 20 ml and 30 ml ethylene glycol (EG) respectively by magnetic stirrer. Then the tin chloride solution was added drop wise into the sodium sulfide solution under stirring condition. The solution turned dark brown colour with the addition of $SnCl_2.2H_2O$ which indicates the formation of SnS particles. The obtained solution was put into a Teflon-lined stainless steel autoclave. Then the autoclave was placed in a furnace at 180 ^{0}C for 18 h and then the solution was allowed to cool down to room temperature

naturally. The obtained product was centrifuged and washed with deionised water for several times. The product is finally dried at 50 ^{0}C for 72 h.

To prepare colloidal silver nanoprticles (Ag), 1.0 gm as prepared PVP was dissolved in 50 ml ethylene glycol (EG). Then 0.1 gm silver nitrate ($AgNO_3$) was added to this solution under slowly stirring condition. The system was then maintained at 120 ^{0}C for 1 h under stirring. Then the prepared colloidal silver solution was cooled to room temperature.

SnS-Ag nanocomposite was prepared by chemical method. To prepare SnS-Ag nanocomposite, 1.13 gm tin chloride solution and 0.39 gm sodium sulfide solution were prepared individually in 15 ml deionised water. Then these two solutions and 20 ml colloidal silver solution are taken in an autoclave. The autoclave is placed in a furnace at 180 ^{0}C for 18 h. After that, the solution was allowed to cool down to room temperature slowly. The final precipitate was centrifuged and washed with deionised water for some times. Finally the product is dried at 60 ^{0}C for few days.

The crystal structure of the samples were performed using X-ray diffractometer by Bruker Axs D2 phaser SSD160 with Cu-kα radiation (λ=1.5405Å) in the range of 20° to 70°. Transmission electron microscopy (TEM) of as prepared samples was carried out by JEOL JEM200 with an operating voltage at 200KV. The surface information of the grown samples has been characterized by FESEM using ZEISS MERLIN6105. The elemental analysis was performed by energy dispersive analysis of X-rays (EDAX). Optical absorption spectra of as grown samples were carried out by Shimadzu- Pharmaspec-1700 UV-VIS spectrophotometer in the optical range 300nm-900nm at room temperature. Photoluminescence spectra of as prepared samples were examined by Perkin Elmer LS55 Fluorescence Spectrometer. Time-Correlated Single Photon Counting (TCSPC) of as prepared samples was measured by Delta flex-01-DD.

3.6.2. Results and discussion

3.6.2.1. XRD study

Fig. 3.38 shows the XRD patterns of as prepared SnS and SnS-Ag nanocomposite using X-ray diffractometer by Bruker Axs D2 phaser SSD160 with Cu-kα radiation (λ=1.5405Å) in the range of 20° to 70°. All these diffraction planes are exactly matched with orthorhombic crystal structure of SnS nanocrystals with lattice parameters $a = 0.432, b = 1.121$ and $c = 0.399$ nm (JCPDS card no: 39-0354). The strong and sharp XRD peaks indicate that the samples are well crystalline. The approximate crystal size has been determined from Debye Scherer formula .The calculated crystal sizes of the as prepared SnS and SnS-Ag were approximately 2.71 nm and 3.56 nm respectively.

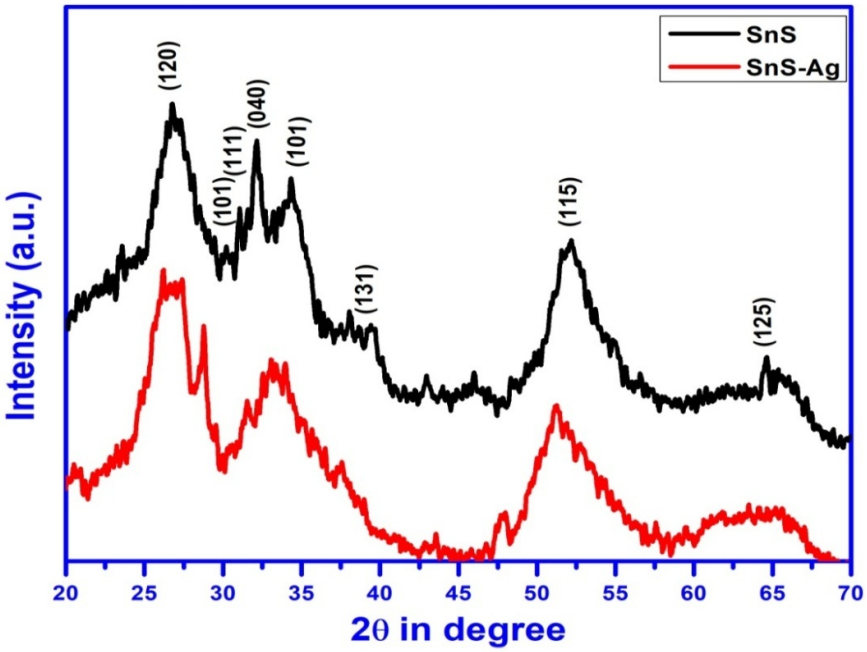

Fig. 3.38. XRD pattern of SnS and SnS-Ag nanocomposite

A peak shift is observed in SnS-Ag nanocomposite compared to the pure SnS nanomaterials. This shift is due to the dopant according to Vigard's law which state that the dopant alone cannot generate individual peak other then the host peak, but can produce adequate shift in the position of host peak [202].

3.6.2.2. TEM study

Transmission Electron Microscopy (TEM) is used to determine Morphology, nature of crystal and crystal size. Fig. 3.39 (a) and 3.39 (b) shows the TEM images (inset SAED) of SnS and SnS-Ag nanocomposite respectively. Quantum dot like particles are observed in both SnS and SnS-Ag nanostructures. The particles are distributed uniformly. The average crystal sizes of SnS and SnS-Ag have been determined using image-J software. The average estimated crystal sizes were close to 5.50 nm and 7.30 nm of SnS and SnS-Ag respectively. Selected area electron diffraction (SAED) pattern indicates the crystalline nature is present.

3.6.2.3. FESEM study

Surface morphology gives the information about the shape and size of the surface particles. The surface images of SnS and SnS-Ag are shown in fig. 3.39 (c,d). FESEM images of SnS and SnS-Ag indicates that the surface morphologies are crystalline nature.

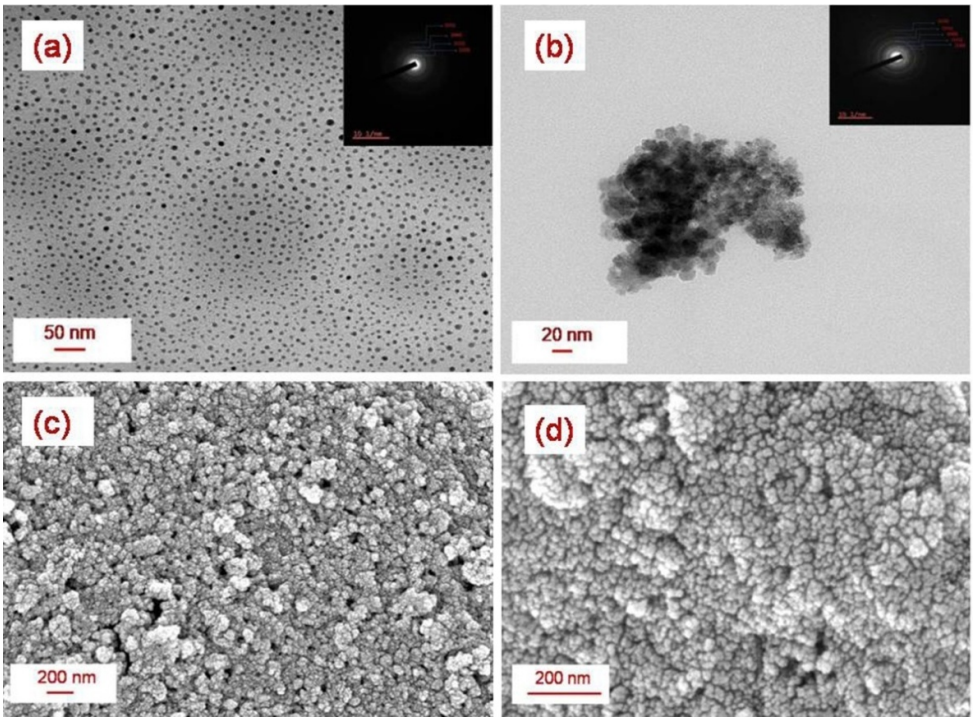

Fig. 3.39. TEM image and SAED (inset) pattern of (a) SnS (b) SnS-Ag; FESEM image of (c) SnS (d) SnS-Ag.

3.6.2.4. EDX study

Electron diffraction X-ray analysis (EDX) finds out the information about constitute element, purity of materials and atomic weight percentages. Fig. 3.40 (a,b) indicates the EDX spectrum of the as prepared samples. From EDX analysis it is seen that the ratio of Sn/S of SnS is 69.01/30.99 and for SnS-Ag is 70.97/25.79. The atomic percentage of Ag was found to be 3.24 (fig. 3.40 c and d). It is clear from EDX analysis the presence of Ag^{2+} cations. Since the stochiometric deviation is quite small, the change in band gap energy is due to the quantum confinement effects [206].

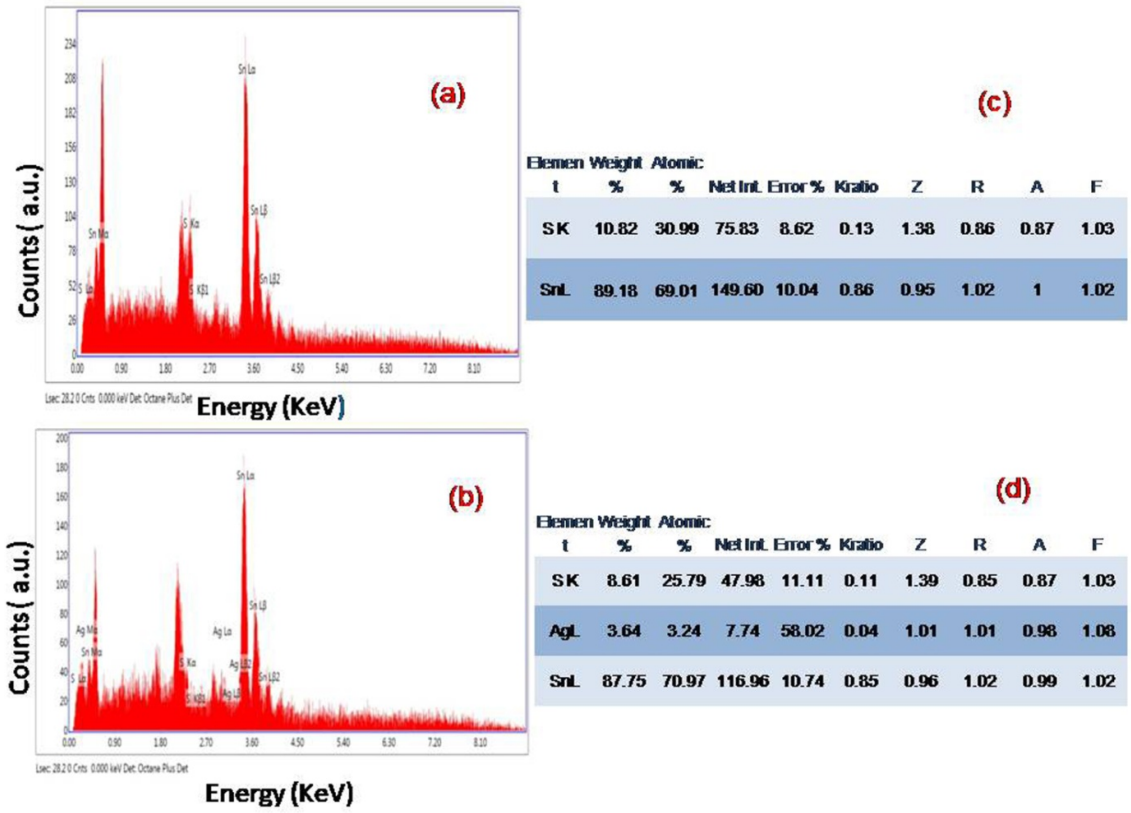

Fig. 3.40. EDAX spectrum of (a) SnS (b) SnS-Ag nanocomposite; Atomic weight percentage of (c) SnS (d) SnS-Ag nanocomposite.

3.6.2.5. UV-VIS spectroscopy study

UV-VIS spectroscopy is a useful measurement to determine band gap energy and to study the optical properties of semiconducting materials. Fig. 3.41 (a) gives the plot of optical

absorption coefficient versus wavelength of incident light in the optical range 300nm-800nm. From optical absorption spectrum it is clear that SnS-Ag nanocomposite is a good absorber in the sun light than SnS nanocrytals. Optical band gap energy of the samples were determined from the relation $(\alpha h\nu)^2 = C\,(h\nu - E_g)$ (3.6.1)

Where C is a constant, E_g is the optical band gap energy of the samples and α is the absorption coefficient of the materials. The variation of $(\alpha h\nu)^2$ vs. photon energy (hν) of the samples is shown in fig. 3.42(b). From these $(\alpha h\nu)^2$ vs. hν curve we calculated the band gap energy which were 2.04 eV and 1.80 eV of SnS and SnS-Ag nanocomposite respectively. A decrease in the band gap energy of SnS-Ag nanocomposite was observed compared to SnS. This decrease in the band gap energy is due to the proscribed impurities which take place in the formation of donor levels within the optical energy gap close to the conduction band and hence it can absorb low energy photon easily [207]. Absorption curve shows a broad peak in the range between 400 nm to 550 nm in case of SnS-Ag nanocomposite. But no such peak is observed in case of pure SnS sample. Hence, this broad peak arises due to the Surface Plasmon Resonance (SPR) which is contributed by the presence of Ag nanoparticles.

3.6.2.6. Photoluminescence spectroscopy study

Photoluminescence is an effective approach to evaluate the defect state or impurity state. Fig. 3.42 (c) shows the PL spectra of SnS and SnS-Ag nanocomposite. The emission peaks arises from 608.19 nm and 696.25 nm of SnS and SnS-Ag nanocomposite respectively. As particle size of SnS-Ag naocomposite increases, the PL peak shift towards the higher wavelength side. This is due to the fact that there is tendency to attach the particles of SnS and Ag at the time of formation of nanocomposite. The emission peak of SnS and SnS-Ag nanocomposite are probably arising from close to the conduction band which is due to the different defect states such as sulfur vacancies, tin ion vacancies etc [46].

3.6.2.7. TCSPC study

Time-Correlated Single Photon Counting (TCSPC) study investigates the PL decay life time of the carriers. A laser source of wavelength 416 nm was used to stimulate the carriers of the samples to the higher energy states. After a few moments these charge carriers returns to the ground state energy level. The following working formula was used to determine the PL decay life time of the carriers

$$\tau_{av} = \sum \frac{\alpha_i \tau_i}{\alpha_i} \qquad (3.6.2)$$

Where $\tau's$ are the decay components and α's are the respective amplitudes of life time components. The PL decay life time of the samples were depicted in fig.3.42 (d).

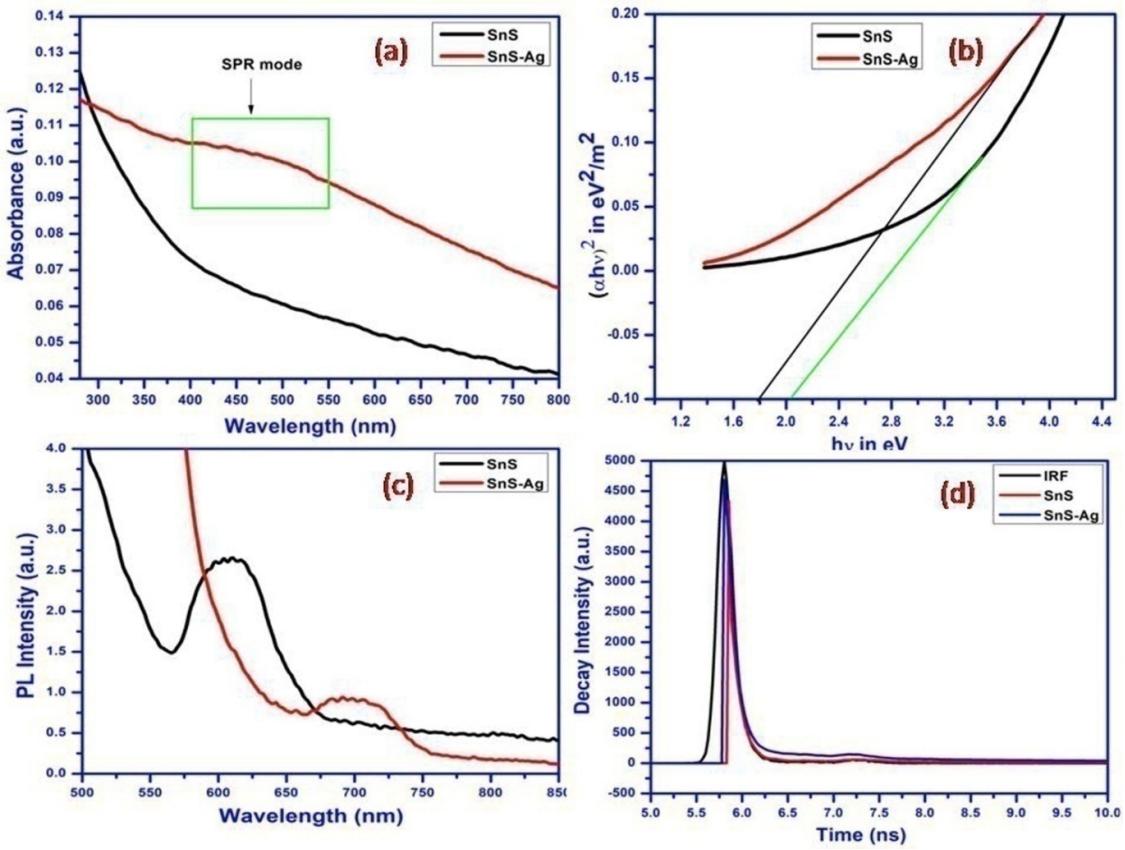

Fig. 3.41. (a) UV-VIS absorption spectra of as prepared SnS and SnS-Ag; (b) Band gap determination curve of SnS and SnS-Ag; (c) PL spectra of as synthesized samples; (d) TCSPC spectra of the samples.

The calculated values of PL decay life time of SnS and SnS-Ag were18.6 ps and 48.6 ps respectively. From TCSPC measurements it is clear that the PL decay life time of SnS is less than the SnS-Ag composite. Smaller is the crystal size, higher is the surface area which results in surface recombination.

Table: 3.7

Results obtained from structural and optical properties of SnS and SnS-Ag nanocomposite

Samples	Pattern	Crystal structure from XRD	Average Crystal size (nm) from TEM image	Surface morphology from FESEM	Band gap (eV) from UV-VIS spectroscopy	PL peak (nm) position	PL decay life time (ps) from TCSPC
Pure SnS	Particle	Orthormbic	5.50	Spherical	2.04	608.19	18.6
SnS-Ag	Particle	Orthormbic	7.30	Spherical	1.80	696.25	48.6

3.6.3. Conclusion

SnS and SnS-Ag nanocomposite were prepared by cost effective solvothermal method. XRD results show that the samples are in orthorhombic structure in phase. TEM results indicate that quantum dot like particles are observed in both SnS and SnS-Ag nanostructures. The crystalline nature is present and is confirmed by SAED. EDAX analysis confirmed that Ag is present in SnS-Ag nanocomposite. From optical absorption study it is clear that SnS-Ag nanocomposite is a good absorber in the sun light than SnS nanocrytals. A decrease in the band gap of SnS-Ag nanocomposite was observed compared to SnS. The PL study indicates that a peak shift of SnS-Ag naocomposites towards the higher wavelength side.

3.7. Green synthesis and Characterization of SnS Nanoparticles using the Extraction of Gymnema Sylvestre leaves

Chemically grown SnS and green synthesized SnS nanoparticles were prepared by simple and cost effective hydrothermal method. The green synthesis was fruitfully utilized to prepare SnS NPs by the Gymnema Sylvestre leaves extract. The leaves extract of Gymnema Sylvestre plant have been employed as an efficient capping agent for the synthesis of SnS NPs. The green synthesized as well as chemically synthesized SnS NPs were characterized in terms of structural, morphology and optical properties using different experimental techniques. The XRD results suggest that the as synthesized SnS NPs are perfectly matched with the orthorhombic crystal structure. From TEM image, the average crystal size of both samples lies in between ~2 nm to ~ 4 nm. EDAX result shows that the stoichiometry ratios of Sn/S of the samples are well maintained. Optical properties of the as prepared samples were characterized through UV-VIS absorption spectroscopy as well as photoluminescence (PL) spectroscopy.

3.7.1. Experimental section

3.7.1.1. Materials

Chemically grown SnS and green synthesized SnS nanoparticles were prepared by simple hydrothermal method. Tin chloride ($SnCl_2.2H_2O$) and Thiourea (CH_4N_2S) were purchased from Merck, India. All materials were used as starting materials without any further purification.

3.7.1.2. Collection and extraction of plant samples

Gymnema Sylvestre fresh leaves were collected from the garden of botany department, Vidyasagar University campus, West Bengal, India. The Fresh leaves of Gymnema Sylvestre plant were washed with double distilled water for many times. These washed leaves were

drying in a vacuum furnace for 2 hours at 40 ^{0}C to take away the moisture. 30 gm of fresh washed, desiccated, small cut leaves were added into 200 mL of distilled water. After that, these leaves are boiled for 45 min until the color of the aqueous solution transforms watery to brownish color. This brownish aqueous solution was filtered and stored at 5^{0}C for further use.

3.7.1.3. Chemically synthesis of SnS NPs

Simple hydrothermal method was followed to synthesized tin sulfide nanoparticles (SnS) nanoparticles. In this growth process, 2.25 gm tin chloride ($SnCl_2.2H_2O$) and 0.76 gm thiourea (CH_4N_2S) were dissolved (ratio 1:1) separately in 40ml deionised water. Then both the solutions are mixed together and stirred for 15 minutes by the magnetic stirrer. After that this solution was taken in a Teflon-lined stainless steel autoclave and placed it into the furnace at 180°C for 18 hours. The obtained solution was then cooled down at room temperature. The black products were centrifuged, washed with deionised water in sequence for many times and dried at room temperature for few days.

3.7.1.4. Green synthesis of SnS NPs

To prepare green synthesized SnS nanoparticles, 50 mL of Gymnema Sylvestre leaves extract was taken in a fresh beaker. At first, 2.25 gm of $SnCl_2.2H_2O$ which is the source of tin was added to the reaction medium. In this typical synthesis process, Gymnema Sylvestre leaves extract has been used as capping agent. Then, 0.76 gm of thiourea, source of sulphur was added to the solution. The mixed solution was stirred for 15 minutes by the magnetic stirrer. After that this solution was taken in a Teflon-lined stainless steel autoclave and placed it into the furnace at 180°C for 18 hours. A brown black colored powder was carefully collected in previous manner and packed for further characterization.

3.7.2. Sample characterization

The phase and the structure of the crystal were carried out by X-ray diffraction (XRD) study of the samples using Bruker Axs D2 phaser SSD160 with Cu-kα radiation (λ=1.5405Å)

within the range 20° to 70°. The morphology of as prepared samples was characterized by Transmission electron microscope (TEM) using JEOL JEM200 operating at 200KV. The surface structure of the prepared samples has been studied by FESEM using ZEISS MERLIN6105. Energy dispersive X-rays analysis (EDAX) measurement has been used to study the chemical compositions of the said samples. UV-VIS absorption studies of samples were done in the wavelength range 200nm-900nm by Shimadzu-Pharmaspec-1700. PL spectra of the nano samples were recorded by Perkin Elmer LS55 Fluorescence Spectrometer.

3.7.3. Results and discussion

3.7.3.1. Structural study

Fig.3.42 demonstrates the X-ray diffraction patter of as prepared chemically grown SnS and green synthesized SnS nanoparticles. XRD study shows a strong sharp peak situated at 31.67^0 consequent to (111) planes of SnS. The observed diffraction peaks are compared with JCPDS data (JCPDS card no: 39-0354). All these reflection peaks have been indexed as the orthorhombic crystal structure of SnS (lattice parameters $a = 0.432, b = 1.121$ and $c = 0.399$ nm).

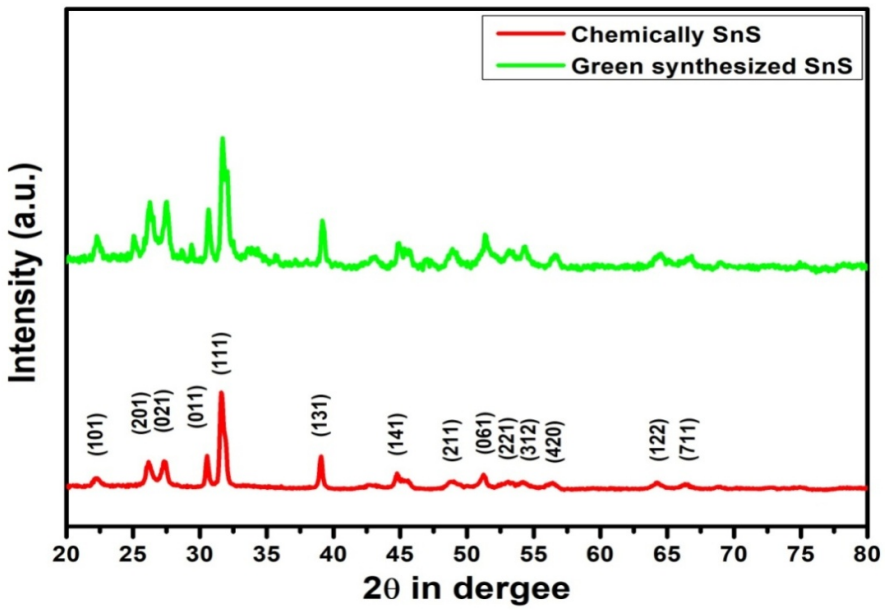

Fig. 3.42. XRD image of chemically grown SnS and green synthesized SnS NPs

No extra XRD peaks were observed. Besides, the well-defined and sharp peaks were observed in the XRD patterns and this indicates the good crystalline nature of SnS NPs. The approximate particle size has been calculated with the help of Debye Scherer's formula. From Debye Scherer formula, the estimated crystal size of chemically grown SnS and green synthesized SnS nanoparticles were found to be 16.30 nm and 15.81 nm respectively.

3.7.3.2. Morphology study

The morphological structure i.e shape and size of the nanocrystals were analysed by transmission electron microscope (TEM) study. Fig. 3.43 (a,b) depicted the TEM image (inset SADE) of as prepared chemically grown SnS as well as green synthesized SnS nanoparticles. The average diameter of the SnS nanocrystals was determined using image-J tools.

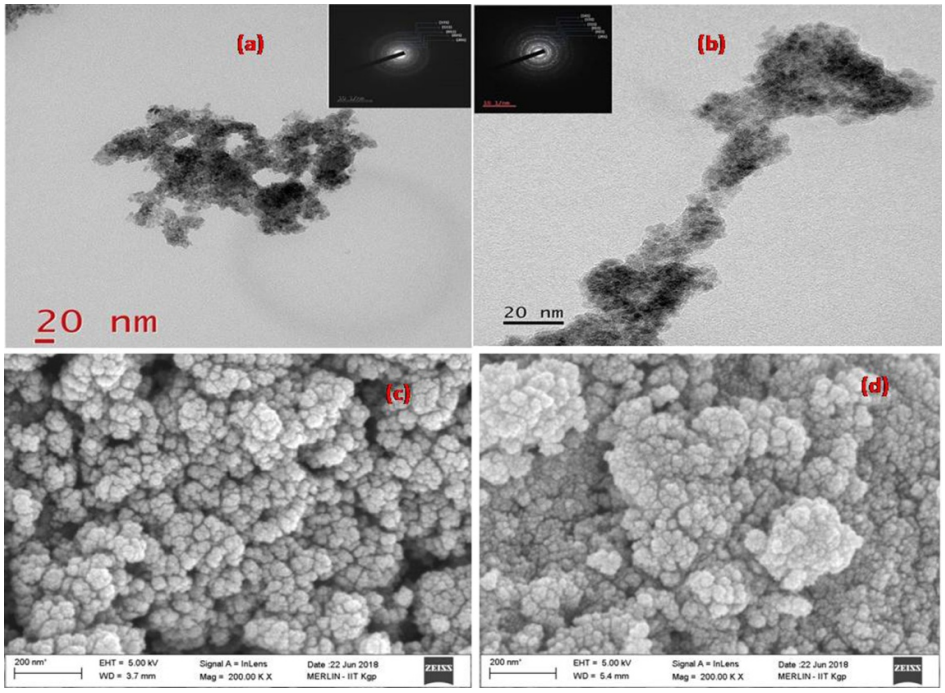

Fig. 3.43. TEM image and SAED (inset) pattern of (a) chemically grown SnS (b) green synthesized SnS; FESEM image of (c) chemically grown SnS (d) green synthesized SnS.

The average diameter of chemically growth SnS and green synthesized SnS nanoparticles were estimated and reported to be 3.98 nm and 2.01nm respectively. From TEM image, it is

clear that average crystal size is small in case of green synthesized SnS with respect to chemically grown SnS. This decrease in particle size in case of green synthesized SnS is probably due to the taken of Gymnema Sylvestre leaves extract as a capping agent [132]. So capping agent is an important fundamental factor to restrict the particle size. Hence we can say that the Gymnema Sylvestre leaves extract is a good capping agent than the ethylene glycol (EG). Selected area electron diffraction (SAED) pattern indicated the crystallinity of SnS NPs.

Field Emission Scanning Electron Microscopy (FESEM) study presents the information about the nature of the particles in surface. Fig. 3.43 (c,d) shows the FESEM images of the as prepared SnS nanocrystals. FESEM results indicated that the surface characteristics of the prepared samples also show particle behaviour.

3.7.3.3. Composition study

Elemental composition and the clarity of the samples were confirmed by Electron Dispersion X-ray Analysis (EDAX). The EDAX spectrum of as prepared chemically grown SnS and green synthesized SnS were represented in fig. 3.44.

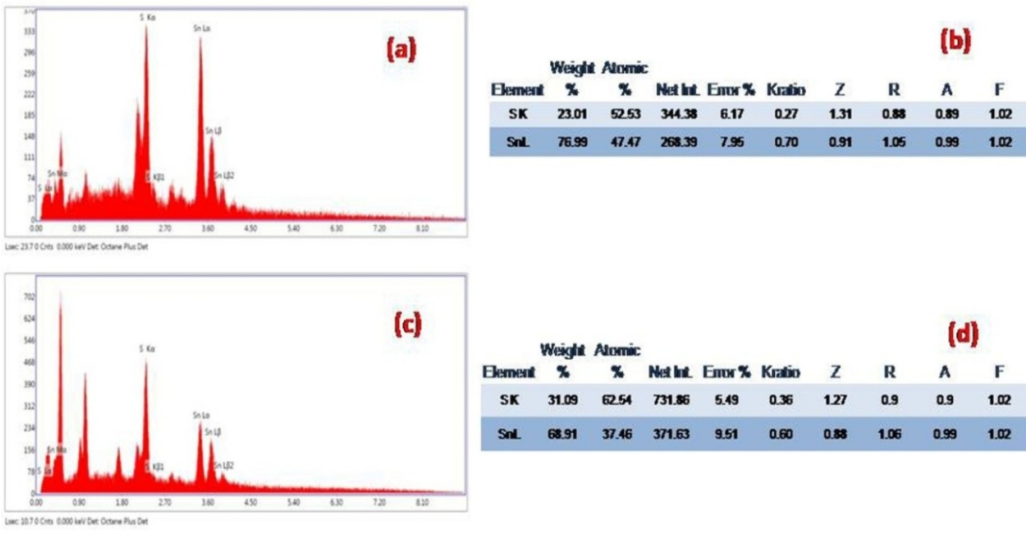

Fig. 3.44. EDAX spectrum and atomic percentage of (a,b) chemically grown SnS; (c,d) green synthesized SnS NPs.

From EDAX analysis is clear that the the stoichiometry of Sn:S is maintained well for chemically grown SnS whereas the sulfur (S) is excess than tin (Sn) for green synthesized SnS. This is probable due to the use of leaves extract as capping agent. The EDAX study presented the ratio of Sn/S of chemically grown SnS is 52.53/47.47 whereas the green synthesized SnS is 62.54/37.46. This is tabulated in table 3.8.

Table: 3.8

Composition of chemically SnS and green synthesized SnS nanoparticles estimated by EDAX analysis

Samples	Sn (at. %)	S (at.%)	Sn/S
Chemically SnS	47.47	52.53	0.90
Green synthesized SnS	37.46	62.54	0.60

3.7.3.4. UV-VIS spectroscopy study

Optical absorption properties of chemically grown SnS and green synthesized SnS have been measured through UV-VIS spectroscopy study in the optical span in between 250 nm to 900 nm. UV-VIS absorbance spectroscopy study determines the quality of absorption in the visible range as well as gives about the band gap information of the materials. UV-VIS absorption spectra show the variation of optical absorbance coefficient with the wavelength of visible light and it is presented in fig. 3.45(a). The direct band gap of the semiconductor nanoparticles have been estimated through the relation

$$(\alpha h\nu)^2 = C(h\nu - E_g) \qquad (3.7.1)$$

where C is a constant. E_g is the optical band gap energy and α is the optical absorption coefficient of the sample. The plot of $(\alpha h\nu)^2$ vs. hν of the nano samples have been depicted in fig.3.45(b,c). The linear portion of the graphs has been extrapolated to energy (hν) axis to determine band gap (E_g). The estimated direct band gap energy of the chemically grown SnS as well as green synthesized SnS were 2.11 eV and 2.27 eV respectively. An increase in the

band gap energy has been observed in green synthesized SnS compared to that of chemically SnS. This is probably due to the decrease in particle size.

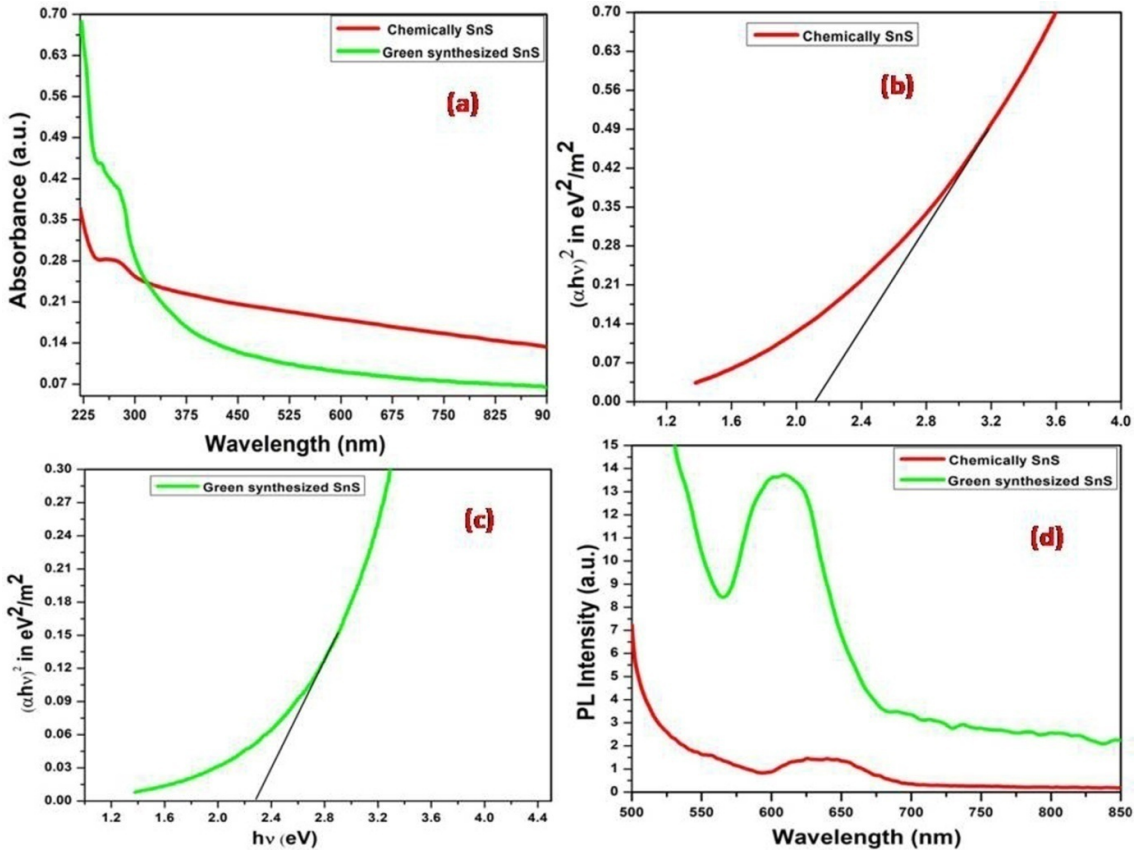

Fig. 3.45. (a) Optical absorption spectra of the samples; Plot of $(\alpha h\nu)^2$ vs. hν of (b) chemically grown SnS (c) green synthesized SnS; (d) Photoluminescence spectra of chemically grown SnS and green synthesized SnS

3.7.3.5. Photoluminescence spectroscopy study

Photoluminescence spectroscopy (PL) properties of as prepared SnS nanoparticles have been studied to analyse the optical response as well as defect state. Fig. 3.45(d) shows the PL spectra of chemically grown SnS and green synthesized SnS nanoparticles. Photoluminescence study indicates the PL peak of green synthesized SnS shifted in the lower wavelength side with respect to chemically grown SnS nanoparticles. Hence, a blue shift occurs in case of green synthesized SnS nanoparticles. An excitation wavelength of 460 nm has been applied. From PL curve it is seen that the emission peaks of chemically grown SnS and green synthesized SnS are arising from 632.01 nm (1.96 eV) and 607.79 nm (2.04 eV)

respectively. Hence, the emission peaks are probably coming from the lower of the conduction band of SnS nanocrystals which is due to the different defect states such as sulfur vacancies and tin ion vacancies [46]. Therefore a blue shift is mainly responsible for the quenching results of the carriers of green synthesized SnS nanocrystals [208]. The structural, morphological and optical characterization of the samples is presented in the table 3.9.

Table: 3.9

Determination of size, shape and band gap of as prepared SnS NP

Name of Sample	Shape of Nanostructure	Crystal structure from XRD	Average Size of the Nanostructure (From TEM) (nm)	Band Gap (eV) measured from UV-vis	PL peak position in nm
Chemically SnS	Nanoparticles	Orthorhombic	Diameter-3.98	2.11	632.01
Green synthesized SnS	Nanoparticles	Orthorhombic	Diameter-2.01	2.27	607.79

3.7.4. Conclusion

The green synthesis was fruitfully utilized to prepare SnS NPs by the Gymnema Sylvestre leaves extract. The leaves extract of Gymnema Sylvestre plant have been employed as an efficient capping agent for the synthesis of SnS NPs. The green synthesized as well as chemically synthesized SnS NPs were characterized in terms of structural, morphology and optical properties. The XRD result shows that the as prepared SnS NPs are perfectly matched with the orthorhombic crystal phase of SnS. The TEM analysis confirms that the particle diameter of green synthesized SnS NPs is less than the chemically synthesized SnS NPs. The particle size of both samples lie in between ~2 nm to ~ 4 nm. UV-VIS absorption study shows that an increase in band gap of green synthesized SnS NPs was observed compared to that of chemically grown SnS NPs. PL study mainly determines the surface states. A blue

shift has been observed in case of green synthesized SnS NPs with respect to chemically grown SnS NPs. Therefore, the novel green synthesis of SnS NPs from the Gymnema Sylvestre leaves extract is a pollutant free and low cost synthesis method.